Atmospheric muon flux at sea level, underground, and underwater

E. V. Bugaev,[1] A. Misaki,[2] V. A. Naumov,[3,4,5] T. S. Sinegovskaya,[4] S. I. Sinegovsky,[4] and N. Takahashi[6]

[1]*Institute for Nuclear Research, Russian Academy of Science, Moscow 117312, Russia*
[2]*National Graduate Institute for Policy Studies, Urawa 338-8570, Japan*
[3]*Laboratory of Theoretical Physics, Irkutsk State University, Irkutsk 664003, Russia*
[4]*Department of Theoretical Physics, Physics Faculty, Irkutsk State University, Irkutsk 664003, Russia*
[5]*Istituto Nazionale di Fisica Nucleare, Sezione di Firenze, Firenze 50125, Italy*
[6]*Department of Electronics and Information System Engineering,*
Faculty of Science and Technology, Hirosaki University, Hirosaki 036-8561, Japan

The vertical sea-level muon spectrum at energies above 1 GeV and the muon intensities at depths up to 18 km w.e. in different rocks and in water are calculated. The results are particularly collated with a great body of the ground-level, underground, and underwater muon data. In the hadron-cascade calculations, we take into account the logarithmic growth with energy of inelastic cross sections and pion, kaon, and nucleon generation in pion-nucleus collisions. For evaluating the prompt-muon contribution to the muon flux, we apply the two phenomenological approaches to the charm production problem: the recombination quark-parton model and the quark-gluon string model. To solve the muon transport equation at large depths of a homogeneous medium, we used a semianalytical method, which allows the inclusion of an arbitrary (decreasing) muon spectrum at the medium boundary and real energy dependence of both continuous and discrete muon energy losses. The method is checked for accuracy by direct Monte Carlo calculation. Whenever possible, we give simple fitting formulas describing our numerical results. [S0556-2821(98)00313-0]

PACS number(s): 13.85.Tp, 96.40.Tv

I. INTRODUCTION

The flux of cosmic-ray muons in the atmosphere, underground, and underwater provides a way of testing the inputs of nuclear cascade models, that is, parameters of the primary cosmic-ray flux (energy spectrum, chemical composition) and particle interactions at high energies. In particular, measurements of the muon energy spectra, angular distributions, and the depth-intensity relation (DIR) have a good potential for yielding information about the mechanism of charm production in hadron-nucleus collisions at energies beyond the reach of accelerator experiments. This information is a subject of great current interest for particle physics [1] and yet is a prime necessity in high-energy and very-high-energy neutrino astronomy [2]. Indeed, the basic and unavoidable background for many future astrophysical experiments with full-size underwater or underice neutrino telescopes will be an effect of the atmospheric neutrino flux of energies from about 1 TeV to tens of PeV. However, in the absence of a generally recognized and tried model for charm hadroproduction, the current estimates of the ν_μ and (most notably) ν_e backgrounds have inadmissibly wide scatter even at multi-TeV neutrino energies, which shoots up with energy. At $E_\nu \sim 100$ TeV, different estimates of the ν_μ and ν_e spectra vary within *a few orders of magnitude* (see Refs. [2–5] for reviews and references).

The present state of the art of predicting the atmospheric neutrino flux seems to be more satisfactory at energies below a few TeV. However, the theory meets more rigid requirements on the accuracy of the calculations here [6]: for an unambiguous treatment of the current data on upgoing (atmospheric neutrino induced) muon flux, the neutrino flux must be calculated with a 10% accuracy at least, whereas the

uncertainties in the required input data (primary spectrum, cross sections for light meson production, etc.) hinder the achievement of these ends. Because of this, a vital necessity is in a normalization of the calculated (model-dependent) atmospheric neutrino flux and the muon flux is perhaps the only tool for such a normalization. The point is that atmospheric muons and neutrinos are generated in just the same processes. Therefore, the accuracy of the neutrino flux calculation can be improved by forcing the poorly known input parameters of the cascade model to fit the data on the muon flux.

The sea-level muon data obtained by direct measurements with magnetic spectrometers are crucial but still insufficient for this purpose. The fact is that numerous sea-level measurements (see, e.g., Refs. [7–17] for the vertical muon flux, Refs. [18,19] for near-horizontal flux, and Ref. [20] for a compilation of the data) are in rather poor agreement with one another, even though each of the experiments by itself typically has very good statistical accuracy. This is true to a greater or lesser extent everywhere over the whole energy region accessible to the ground-based installations.

On the other hand, a quite representative array of data on cosmic-ray muon DIR in rock and, to a lesser extent, in water has been accumulated. Underground muon experiments may number in the tens in a span of 60 years (see Refs. [21–46] and also [47–49] for reviews and further references). It should be noted that the results of many early measurements, specifically those performed at shallow depths, have not lost their significance today, considering that modern experiments principally aim at greater depths. Underwater muon experiments have over 30 years of history [50–57] and it is believed that they will gain in importance with the progress of high-energy neutrino telescopes.

It may be somewhat unexpected but the underground data are more self-consistent in comparison with ground-level data, at least for depths to about 6 km of water equivalent (w.e.) (corresponding roughly to 3–4 TeV of muon energy at sea level) and hence they provide a useful check on nuclear cascade models. There is a need to piece together all these data in order to extract some physical inferences thereof. Also, it would be useful to correlate the underground and underwater data with the results of the mentioned direct measurements of the sea-level muon spectrum [7–17] as well as with the data deduced by indirect routes [33,36,37,44,58–64].

It is the purpose of this paper to discuss the above-mentioned data on the vertical muon flux at sea level, underground, and underwater in the context of a single calculation, with emphasis on the prompt-muon problem. The implementation of the results to the normalization of the high-energy atmospheric neutrino flux will be discussed elsewhere [65].

In Sec. II we discuss the model employed for the primary spectrum and composition as well as the nuclear-cascade model for production and propagation of high-energy nucleons, pions, and kaons in the atmosphere. Some required formulas for the atmospheric muon flux are given in Sec. III; at the end of that section, we give a simple parametrization for the calculated vertical spectrum of conventional (π,K) muons at sea level. The models for charm hadroproduction, those used in the present work to make an estimate of the prompt-muon (PM) contribution, are the concern of Sec. IV; the recombination quark-parton model is considered in some detail. We also give the model formulas for the muon spectra from the inclusive semileptonic decays of a D meson and Λ_c hyperon in the laboratory frame. At the end of this section, we present simple parametrizations for the predicted differential and integral PM spectra. In Sec. V we compare our predictions for the vertical muon spectra (differential and integral) with the direct and indirect data at sea level. Section VI is concerned with muon propagation through matter. Calculation of the muon intensity at large depths is a rather nontrivial problem even though the muon energy spectrum at the medium boundary is assumed to be known; we briefly sketch our semianalytical approach to that problem. The comparison between the calculated muon DIR and the afore-cited underground and underwater data is fully considered in Sec. VII. Our conclusions are presented in Sec. VIII.

II. NUCLEAR-CASCADE MODEL

A. Primary spectrum and composition

For energies above 1 TeV we use the semiempirical model for the integral primary spectrum proposed by Nikol'sky, Stamenov, and Ushev [66] (NSU):

$$F(\geqslant E_0) = F_0 E_0^{-\gamma} \sum_A B_A \left(1 + \delta_A \frac{E_0}{A}\right)^{-\mathscr{æ}}. \quad (2.1)$$

Here E_0 is the energy per particle in GeV, $F_0 = 1.16$ cm^{-2} s^{-1} sr^{-1}, $\gamma = 1.62(\pm 0.03)$, and $\mathscr{æ} = 0.4$. The δ_A's specify the region of the ''knee'' in the primary spectrum. We adopt $\delta_p = 6 \times 10^{-7}$ and $\delta_{A \geqslant 4} = 10^{-5}$. These values correspond to the hypothesis which attributes the change

in the energy spectrum of the primaries at $E_0 \gtrsim 10^3$ TeV to photodisintegration of nuclei with pion photoproduction by photons with energy ~ 70 eV inside the cosmic-ray sources. The chemical composition is given with the following values for B_A: $B_1 = 0.40(\pm 0.03), B_4 = 0.21(\pm 0.03), B_{15} = 0.14 (\pm 0.03), B_{26} = 0.13(\pm 0.03)$, and $B_{51} = 0.12(\pm 0.04)$ for the five standard groups of nuclei. The numerical values of A indicate the average atomic weights in the groups. The corresponding differential spectrum is given by

$$\frac{dF}{dE_0} = \gamma F_0 E_0^{-(\gamma+1)} \sum_A B_A \left(1 + \delta_A \frac{E_0}{A}\right)^{-\mathscr{æ}}$$

$$\times \left[1 + \frac{\mathscr{æ}\,\delta_A E_0/A}{\gamma(1 + \delta_A E_0/A)}\right]. \quad (2.2)$$

The NSU approximation has been deduced from an analysis of fluctuations in the relative number of electrons and muons in extensive air showers and corresponds to the data on absolute intensities of primary protons and various nuclei at energies $E_0 \geqslant 1, 10^3, 10^6$ TeV/particle, and also to the data on the shape of the integral spectrum in the vicinity of the knee (see Ref. [66] for specific sources of the data).

The model, on the whole, fits the modern data on the primary spectrum and composition from about 100 GeV/particle up to 100 EeV/particle. Specifically, at $E_0 \lesssim 10^3$ TeV/particle, the model fits reasonably well the recent results of the COSMOS satellite experiment [67], the JACEE balloon experiment [68], and the BASJE air-shower experiment [69]. On the other hand, there is a strong discrepancy between the NSU model and the recent data of the Japan balloon-borne emulsion chamber experiment [70], which indicates a milder knee shape than that found in the previous experiments, although the data of Ref. [70] for the nuclear composition agree with the NSU model at $E_0 \gtrsim 10$ TeV/particle. The data for the spectrum and composition are most inconsistent in the vicinity of the knee [(10^2-10^4) TeV/particle]. Scanty experimental data favor a pure proton composition at $E_0 \gtrsim 10^4$ TeV/particle rather than the almost fixed composition predicted by the NSU model. In connection it should be noted that an essential contribution to the deep underground flux of muons, in particular, ones originating from the decay of charmed hadrons (at depths below ~ 10km w.e.), is given by the primaries with energies from the knee region. Thus the long-standing problem of the knee is closely allied to the PM problem. At the same time, the total intensity of underground and underwater muons is scarcely affected by the region $E_0 \gg 10^4$ TeV/particle. Thus we will not discuss here the problem of the primary spectrum and composition at superhigh energies (see Refs. [69,71] for current reviews).

B. Nuclear cascade at high energies: Basic assumptions

Our nuclear-cascade calculations at high energies are based on the analytical model of Ref. [72] which describes well all available experimental data on hadron spectra for various atmospheric depths and for energies from about 1 TeV up to about 600 TeV. The processes of regeneration and overcharging of nucleons and charged pions, as well as pro-

duction of kaons, nucleons, and charmed particles in pion-nucleus collisions have been properly accounted for. Let us outline the basic assumptions of the model.

(i) The nuclear component of the primary spectrum is replaced with a superposition of free nucleons. Equation (2.2), transforming to the equivalent nucleon spectrum, yields the following differential energy spectra of protons and neutrons:

$$\frac{dF_p}{dE_N} \equiv \mathcal{D}_p^0(E_N) = \mathcal{D}_1(E_N) + \frac{1}{2}\sum_{A \geqslant 4}\mathcal{D}_A(E_N),$$

$$\frac{dF_n}{dE_N} \equiv \mathcal{D}_n^0(E_N) = \frac{1}{2}\sum_{A \geqslant 4}\mathcal{D}_A(E_N).$$

Here E_N is the nucleon energy (in GeV),

$$\mathcal{D}_A(E_N) = \frac{C_A\mathcal{D}_0 E_N^{-(\gamma+1)}}{(1+\delta_A E_N)^{\ae}}\left[1 + \frac{\ae\,\delta_A E_N}{\gamma(1+\delta_A E_N)}\right],$$

$\mathcal{D}_0 = \gamma B_1 F_0 = 0.75$ cm^{-2} s^{-1} sr^{-1}(GeV/nucleon)$^{-1}$, and $C_A = A^{1-\gamma}B_A/B_1(A=1,4,15,26,51)$. Outside the knee region we use the asymptotic formulas

$$\mathcal{D}_A(E_N) = \begin{cases} C_A\mathcal{D}_0 E_N^{-(\gamma+1)} & \text{for} \quad E_N \ll E_N^{(1)}, \\ 1.25\delta_A^{-\ae}C_A\mathcal{D}_0 E_N^{-(\gamma+\ae+1)} & \text{for} \quad E_N \gg E_N^{(2)}, \end{cases}$$
$$(2.3)$$

where $E_N^{(1)} = 6.5/\delta_A$ GeV/nucleon and $E_N^{(2)} = 0.6/\delta_A$ GeV/nucleon. A numerical procedure is applied to smooth out the calculated spectra of secondary hadrons at energies around the knee region.

(ii) We assume a logarithmic growth with energy of the total inelastic cross sections $\sigma_{iA}^{\text{inel}}$ for interactions of a hadron i with a nuclear target A. Such a dependence arises from a model for the elastic amplitude of hadron-hadron collisions, based on the conception of a double Pomeron with a super-critical intercept [72]. For simplicity's sake we will use also another consequence of this model: the asymptotic equality of the inelastic cross sections for any hadron. Thereby

$$\sigma_{iA}^{\text{inel}}(E) = \sigma_{iA}^0 + \sigma_A\ln\left(\frac{E}{E_1}\right) \quad (i=N,\pi,K,\dots) \quad (2.4)$$

at $E \geqslant E_1 = 1$ TeV. The following values of the parameters are adopted: $\sigma_A = 19$ mb, $\sigma_{NA}^0 = 275$ mb $(N=p,n)$, $\sigma_{\pi^\pm A}^0 = 212$ mb, and $\sigma_{KA}^0 = 183$ mb $(K=K^\pm,K^0,\bar{K}^0)$.

(iii) It is assumed that Feynman scaling holds in the fragmentation region of the inclusive processes $iA \to fX$, where $i=p,n,\pi^\pm$, $f=p,n,\pi^\pm,K^\pm,K^0,\bar{K}^0$, and A is the ''air nucleus.'' So the normalized invariant inclusive cross sections $(E/\sigma_{iA}^{\text{inel}})d^3\sigma_{iA\to fX}/d^3p$ are energy independent at large x (where x is the ratio of the final particle energy to that of the initial one). Let us denote

$$\mathcal{W}_{fi}(x) = \frac{\pi}{\sigma_{iA}^{\text{inel}}}\int_0^{(p_T^{\max})^2}\frac{E}{p_L}\left(E\frac{d^3\sigma_{iA\to fX}}{d^3p}\right)dp_T^2.$$

TABLE I. Fractional moments $Z_{fi}(\gamma)$ of inclusive distributions of nucleons, pions, and kaons for the two values of γ.

i	p	n	π^+	f π^-	K^+	K^-	K_L^0
				$\gamma=1.62$			
p	0.1990	0.0763	0.0474	0.0318	0.0067	0.0023	0.0045
π^+	0.0070	0.0060	0.1500	0.0552	0.0120	0.0120	0.0100
				$\gamma=2.02$			
p	0.1980	0.0585	0.0257	0.0162	0.0039	0.0012	0.0026
π^+	0.0060	0.0040	0.1480	0.0346	0.0100	0.0100	0.0080

Then the fractional moments (''Z factors'') defined by

$$Z_{fi}(\gamma) = \int_0^1 x^{\gamma-1}\mathcal{W}_{fi}(x)dx \quad (2.5)$$

are constant inside the regions with constant exponent γ (that is, outside the knee energy region in the primary spectrum). Table I shows fractional moments $Z_{fi}(\gamma)$ for the two values of γ in the case where the incident particle i is a proton or π^+ meson and $f=p,n,\pi^\pm,K^\pm,K_L^0$. The moments for $i=n$ and π^- can be derived using the well-known isotopic relations for the inclusive cross sections. To calculate the Z factors for all reactions except $\pi A\to NX$ and $\pi A\to KX$, we used a parametrization of CERN Intersecting Storage Rings (ISR) data put forward by Minorikawa and Mitsui [73]. The quantities $Z_{N\pi}$ and $Z_{K\pi}$ were calculated from the two central moments $\langle x\rangle$ and $\langle x^2\rangle$ for the inclusive distributions obtained by Anisovich et al. [74] in the framework of the quasinuclear quark model.

(iv) The kaon regeneration (i.e., the processes $K^\pm A \to K^\pm X$, $K^\pm A\to K^0X$, etc.) is disregarded in our calculations. Also, we neglect the nucleon and pion production in kaon-nucleus collisions as well as pion production in kaon decays, which makes it possible to split up the total system of the transport equations into a nucleon-pion part and a kaon one. Our estimations show that the inclusion of the aforementioned effects will cause the muon flux to increase, but no more than by a few percent. It is clear that similar effects for charmed particles are completely negligible.

(v) At the stage of nuclear cascade (but, of course, not at the muon production stage) the decay of $\pi^\pm$ mesons (critical energy $E_\pi^{\text{cr}}\simeq 0.12$ TeV) is neglected for directions close to vertical at pion energies $\gtrsim 1$ TeV. This approximation greatly simplifies the description of the pion regeneration and the production of nucleons, kaons, and charmed particles in pion-nucleus collisions.

C. Nucleon-pion cascade equations

In line with the above-listed assumptions, the 4×4 system of transport equations for the nucleon-pion part of the cascade can be written

$$\left[\frac{\partial}{\partial h} + \frac{1}{\lambda_i(E)}\right]\mathcal{D}_i(E,h) = \sum_j\frac{1}{\lambda_j^0}\int_0^1\mathcal{W}_{ij}(x)\mathcal{D}_j\left(\frac{E}{x},h\right)\frac{dx}{x^2}$$
$$(2.6)$$

$(i,j=p,n,\pi^+,\pi^-)$, with the boundary conditions

$$\mathcal{D}_p(E,0)=\mathcal{D}_p^0(E), \quad \mathcal{D}_n(E,0)=\mathcal{D}_n^0(E),$$

$$\mathcal{D}_{\pi^+}(E,0)=\mathcal{D}_{\pi^-}(E,0)=0.$$

Here $\mathcal{D}_i(E,h)$ is the differential energy spectrum of particles i at the atmospheric depth h,

$$\lambda_i(E)=\frac{1}{N_0\sigma_{iA}^{\text{inel}}(E)}, \quad \lambda_i^0=\frac{1}{N_0\sigma_{iA}^0},$$

and N_0 is the number of target nuclei in 1 g of air.

The solution to the system (2.6) can be found as an expansion in powers of the dimensionless parameter h/λ_A, where $\lambda_A=1/(N_0\sigma_A)\simeq14.5\lambda_N^0$. Within the power-behaved regions of the primary spectrum described by Eq. (2.3), the solution is of the form

$$\mathcal{D}_p(E,h)=\frac{1}{2}[N^+(E,h)+N^-(E,h)],$$

$$\mathcal{D}_n(E,h)=\frac{1}{2}[N^+(E,h)-N^-(E,h)],$$

$$\mathcal{D}_{\pi^+}(E,h)=\frac{1}{2}[\Pi^+(E,h)+\Pi^-(E,h)],$$

$$\mathcal{D}_{\pi^-}(E,h)=\frac{1}{2}[\Pi^+(E,h)-\Pi^-(E,h)],$$

where

$$N^\kappa(E,h)=\frac{\mathcal{D}_p^0(E)+\kappa\mathcal{D}_n^0(E)}{2j^\kappa}\sum_{\kappa'}(j^\kappa+\kappa')$$

$$\times\exp\left[-\frac{h}{\Lambda_{N\pi}^{\kappa\kappa'}(E)}\right]\left[1+\mathcal{O}\left(\frac{h}{\lambda_A}\right)\right],$$

$$\Pi^\kappa(E,h)=\frac{\mathcal{D}_p^0(E)+\kappa\mathcal{D}_n^0(E)}{2j^\kappa}Z_{\pi N}^\kappa(\gamma)\left(\frac{\Lambda_\kappa}{\lambda_N^0}\right)$$

$$\times\sum_{\kappa'}(-\kappa')\exp\left[-\frac{h}{\Lambda_{N\pi}^{\kappa\kappa'}(E)}\right]\left[1+\mathcal{O}\left(\frac{h}{\lambda_A}\right)\right],$$

$$\frac{1}{\Lambda_{N\pi}^{\kappa\kappa'}(E)}=\frac{1+\kappa'j^\kappa(E)}{2\Lambda_N^\kappa(E)}+\frac{1-\kappa'j^\kappa(E)}{2\Lambda_\pi^\kappa(E)} \quad (\kappa,\kappa'=\pm),$$

$$j^\kappa(E)=\sqrt{1+\frac{Z_{\pi N}^\kappa Z_{N\pi}^\kappa\Lambda_\kappa^2}{\lambda_N^0\lambda_\pi^0}}\simeq1+\frac{Z_{\pi N}^\kappa Z_{N\pi}^\kappa\Lambda_\kappa^2}{2\lambda_N^0\lambda_\pi^0},$$

$$\frac{1}{\Lambda_\kappa}=\frac{1-Z_{NN}^\kappa}{2\lambda_N^0}-\frac{1-Z_{\pi\pi}^\kappa}{2\lambda_\pi^0}, \quad \frac{1}{\Lambda_i^\kappa(E)}=\frac{1}{\lambda_i(E)}-\frac{Z_{ii}^\kappa}{\lambda_i^0},$$

$$Z_{NN}^\kappa=Z_{pp}+\kappa Z_{np}, \quad Z_{\pi\pi}^\kappa=Z_{\pi^+\pi^+}+\kappa Z_{\pi^+\pi^-},$$

$$Z_{\pi N}^\kappa=Z_{\pi^+p}+\kappa Z_{\pi^+n}, \quad Z_{N\pi}^\kappa=Z_{p\pi^+}+\kappa Z_{p\pi^-}.$$

The functions $\Lambda_{N\pi}^{\kappa\kappa'}(E)$ can be treated as the generalized absorption lengths. Not counting the processes of nucleon-antinucleon pair production by pions, the formulas for $\Lambda_{N\pi}^{\kappa\kappa'}(E)$ are very simple:

$$\Lambda_{N\pi}^{\kappa+}(E)=\Lambda_N^\kappa(E), \quad \Lambda_{N\pi}^{\kappa-}(E)=\Lambda_\pi^\kappa(E),$$

and thus

$$N^\kappa(E,h)\propto\exp\left[-\frac{h}{\Lambda_N^\kappa(E)}\right],$$

$$\Pi^\kappa(E,h)\propto\exp\left[-\frac{h}{\Lambda_\pi^\kappa(E)}\right]$$

$$-\exp\left[-\frac{h}{\Lambda_N^\kappa(E)}\right].$$

The $\mathcal{O}(h/\lambda_A)$ corrections were calculated in Ref. [72] and it was demonstrated that they became important at $h>500$–600 g/cm^2. However, these corrections are of no significance for the present purposes, because the greater part of the atmospheric muon flux is generated at the depths $h\lesssim300$ g/cm^2.

D. Kaon production and transport

Kaon decay cannot be neglected even at very high energies; as a result the differential energy spectra of kaons, $\mathcal{D}_K(E,h,\vartheta)$, depend on the zenith angle ϑ. In line with approximation (iv) of Sec. II B and assuming isothermality of the atmosphere, the transport equation for kaons may be written as

$$\left[\frac{\partial}{\partial h}+\frac{1}{\lambda_K(E)}+\frac{E_K^{\text{cr}}(\vartheta)}{Eh}\right]\mathcal{D}_K(E,h,\vartheta)=G_K(E,h)$$

$$(K=K^\pm,K_L^0), \quad (2.7)$$

where $E_K^{\text{cr}}(\vartheta)=m_\mu H_0\sec\vartheta/\tau_\mu$ is the kaon critical energy (at $\vartheta\lesssim75°$), m_K and τ_K are the kaon mass and lifetime, and $H_0\simeq6.44$ km is the parameter of the isothermal atmosphere.

The source function $G_K(E,h)$ describes kaon production in NA and πA collisions. Taking into account the explicit form of the nucleon and pion spectra outside the knee region (see Sec. II C), we have

$$G_K(E,h) = \sum_{i=p,n,\pi^+,\pi^-} \frac{1}{\lambda_i^0} \int_0^1 \mathcal{W}_{Ki}(x) \mathcal{D}_i\left(\frac{E}{x},h\right) \frac{dx}{x^2}$$

$$\simeq \frac{1}{2} \sum_\kappa \left[\frac{Z_{KN}^\kappa(\gamma_h)}{\lambda_N^0} N^\kappa(E,h) + \frac{Z_{K\pi}^\kappa(\gamma_h)}{\lambda_\pi^0} \Pi^\kappa(E,h) \right],$$

$$(2.8)$$

where

$$Z_{KN}^\kappa(\gamma_h) = Z_{Kp}(\gamma_h) + \kappa Z_{Kn}(\gamma_h),$$

$$Z_{K\pi}^\kappa(\gamma_h) = Z_{K^+\pi^+}(\gamma_h) + \kappa Z_{K^+\pi^-}(\gamma_h),$$

and $\gamma_h = \gamma + h/\lambda_A$.

Upon integrating Eq. (2.7) with the source function (2.8) and neglecting the weak h dependence of the kaon Z factors we obtain

$$\mathcal{D}_K(E,h,\vartheta) = \int_0^h \exp\left[-\frac{(h-h')}{\lambda_K(E)} \right] \left(\frac{h'}{h}\right)^{E_K^{cr}(\vartheta)/E} G_K(E,h') dh'$$

$$\simeq \Gamma(\varepsilon_K(\vartheta)) \exp\left[-\frac{h}{\lambda_K(E)} \right]$$

$$\times \sum_\kappa \left[Z_{KN}^\kappa(\gamma) \left(\frac{h}{\lambda_N^0}\right) N_K^\kappa(E,h,\vartheta) + Z_{K\pi}^\kappa(\gamma) \right.$$

$$\left. \times \left(\frac{h}{\lambda_\pi^0}\right) \Pi_K^\kappa(E,h,\vartheta) \right],$$

$$(2.9)$$

$$N_K^\kappa(E,h,\vartheta) = \frac{\mathcal{D}_p^0(E) + \kappa \mathcal{D}_n^0(E)}{4j^\kappa} \sum_{\kappa'} (j^\kappa + \kappa')$$

$$\times \overset{*}{\gamma}\left(\varepsilon_K(\vartheta), \frac{h}{\Lambda_K^{\kappa\kappa'}(E)} \right) \left[1 + \mathcal{O}\left(\frac{h}{\lambda_A}\right) \right],$$

$$\Pi_K^\kappa(E,h,\vartheta) = \frac{\mathcal{D}_p^0(E) + \kappa \mathcal{D}_n^0(E)}{4j^\kappa} Z_{\pi N}^\kappa(\gamma) \left(\frac{\Lambda_\kappa}{\lambda_N^0}\right)$$

$$\times \sum_{\kappa'} (-\kappa') \overset{*}{\gamma}\left(\varepsilon_K(\vartheta), \frac{h}{\Lambda_K^{\kappa\kappa'}(E)} \right)$$

$$\times \left[1 + \mathcal{O}\left(\frac{h}{\lambda_A}\right) \right].$$

Here $\varepsilon_K(\vartheta) = E_K^{cr}(\vartheta)/E + 1$, Γ is the gamma function, $\overset{*}{\gamma}$ is the incomplete gamma function,

$$\overset{*}{\gamma}(\varepsilon,z) = \frac{1}{\Gamma(\varepsilon)} \int_0^1 t^{\varepsilon-1} e^{-zt} dt,$$

and

$$\frac{1}{\Lambda_K^{\kappa\kappa'}(E)} = \frac{1}{\Lambda_{N\pi}^{\kappa\kappa'}(E)} - \frac{1}{\lambda_K(E)}.$$

The approximate solution (2.9) is valid at $E \lesssim 40$ TeV (with $\gamma = 1.62$) and $E \gtrsim 2 \times 10^3$ TeV (with $\gamma = 2.02$). The $\mathcal{O}(h/\lambda_A)$ corrections are small at $h \lesssim 500$ g/cm^2 and the derived solution will suffice for our purpose.

E. Nuclear cascade at low and intermediate energies

For the "low-energy part" of the nuclear cascade ($E_0 \lesssim 1$ TeV/particle), we adopt the relevant results of Refs. [75,76] obtained within a rather circumstantial nuclear-cascade model. The model includes the effects of strong scaling violation in hadron-nucleus and nucleus-nucleus collisions, ionization energy losses of charged particles, temperature gradient of the stratosphere, geomagnetic cut-offs, and solar modulation of the primary spectrum. The computational results were verified considering a great body of data on secondary nucleons, mesons, and muons in wide ranges of geographical latitudes and altitudes in the atmosphere. The model was also tested using low-energy data on contained events observed with several underground neutrino detectors.

Since the key features of the model were discussed in several papers (see, e.g., Ref. [6] and references therein), we shall not dwell upon the question here. Only one point needs to be made. The geomagnetic effects for the sea-level muon flux are sizable up to about 5 GeV. However, later on, we are going to deal with muon data at high latitudes that are insensitive to the geomagnetic cutoff. The same is all the more true of solar modulation effects.

III. CONVENTIONAL MUON FLUX

Our calculation of the muon production and propagation through the atmosphere is based on the standard continuous loss approximation. Our interest is in the muon flux at momenta $p \gtrsim 1$ GeV/c. Thus the $\mathcal{O}(m_\mu^2/p^2)$ effects can be neglected. For simplicity, the nonisothermality of the atmosphere will be ignored in the formulas which follow (see Ref. [76] for the corresponding corrections).

Let $\mathcal{D}_\mu(E,h,\vartheta)$ be the differential energy spectrum of muons at depth h and zenith angle ϑ and $\beta_\mu(E) = -dE/dh = a_\mu(E) + b_\mu(E)E$ be the rate of the muon energy loss due to ionization [$a_\mu(E)$] and radiative and photonuclear interactions in the air [$b_\mu(E)E$]. The muon transport equation is

$$\left[\frac{\partial}{\partial h} + \frac{E_\mu^{cr}(\vartheta)}{Eh} \right] \mathcal{D}_\mu(E,h,\vartheta) = \frac{\partial}{\partial E} [\beta_\mu(E) \mathcal{D}_\mu(E,h,\vartheta)]$$

$$+ G_\mu^{\pi,K}(E,h,\vartheta), \quad (3.1)$$

with

TABLE II. Parameters of the fitting formula (3.4) for the vertical energy spectrum of conventional muons at sea level.

Momentum range (GeV/c)	C (cm^{-2} s^{-1} sr^{-1} GeV^{-1})	γ_0	γ_1	γ_2	γ_3
1–9.2765×10^2	2.950×10^{-3}	0.3061	1.2743	-0.2630	0.0252
9.2765×10^2–1.5878×10^3	1.781×10^{-2}	1.7910	0.3040	0	0
1.5878×10^3–4.1625×10^5	1.435×10^1	3.6720	0	0	0
$>4.1625\times10^5$	10^3	4	0	0	0

$$G_\mu^{\pi,K}(E,h,\vartheta)=\sum_{M=\pi^\pm,K^\pm} B(M_{\mu2})\frac{E_M^{cr}(\vartheta)}{hE}\left(1-\frac{m_\mu^2}{m_M^2}\right)^{-1}$$

$$\times\int_{m_\mu^2/m_M^2}^1 \mathcal{D}_M\left(\frac{E}{x},h,\vartheta\right)dx$$

$$+\sum_{K=K^\pm,K_L^0} B(K_{\mu3})\frac{E_K^{cr}(\vartheta)}{hE}$$

$$\times\int_{x_K^-}^{x_K^+} F_K^\mu(x)\mathcal{D}_K\left(\frac{E}{x},h,\vartheta\right)dx. \tag{3.2}$$

Here $E_\mu^{cr}(\vartheta)=m_\mu H_0\sec\vartheta/\tau_\mu\simeq1.03\sec\vartheta$ GeV is the muon critical energy, $B(M_{\mu2(3)})$ are the branching ratios for the $\pi_{\mu2}$, $K_{\mu2}$, and $K_{\mu3}$ decays, $F_K^\mu(x)$ is the muon spectral function for $K_{\mu3}$ decay, and

$$x_K^\mp=2m_\mu^2[(m_K^2-m_\pi^2+m_\mu^2)$$
$$\pm\sqrt{(m_K^2-m_\pi^2+m_\mu^2)^2-4m_\mu^2 m_K^2}]^{-1}.$$

The explicit form of $F_K^\mu(x)$ is rather cumbersome but there is no need to write it out because the $K_{\mu3}$ decay contribution to the muon flux does not exceed 2.5% [77].

The solution to Eq. (3.1) is given by

$$\mathcal{D}_\mu(E,h,\vartheta)=\int_0^h W_\mu(E,h,h',\vartheta)$$

$$\times G_\mu^{\pi,K}(\mathcal{E}(E,h-h'),h',\vartheta)dh'.$$

Here

$$W_\mu(E,h,h',\vartheta)=\frac{\beta_\mu(\mathcal{E}(E,h-h'))}{\beta_\mu(E)}$$

$$\times\exp\left[-\int_{h'}^h\frac{E_\mu^{cr}(\vartheta)}{\mathcal{E}(E,h-h'')}\frac{dh''}{h''}\right] \tag{3.3}$$

and $\mathcal{E}(E,h)$ is the root of the integral equation

$$\int_E^\mathcal{E}\frac{dE}{\beta_\mu(E)}=h,$$

that is, the energy which a muon must have at the top of the atmosphere in order to reach depth h with energy E. As our analysis demonstrates, the weak (logarithmic) energy dependence of the functions a_μ and b_μ is only essential for near-

horizontal directions and can be disregarded with an accuracy better than 3% for directions close to vertical. In this approximation,

$$\mathcal{E}(E,h)=\left(E+\frac{a_\mu}{b_\mu}\right)\exp(b_\mu h)-\frac{a_\mu}{b_\mu}$$

and

$$\frac{\beta_\mu(\mathcal{E}(E,h))}{\beta_\mu(E)}=\exp(b_\mu h).$$

In numerical calculations we use $a_\mu=2.0$ MeV cm^2/g and $b_\mu=3.5\times10^{-6}$ cm^2/g. Equation (3.3) can be simplified in the two particular cases. At $E\gg E_\mu^{cr}(\vartheta)$ the muon decay can be neglected, and so

$$W_\mu(E,h,h',\vartheta)\simeq\exp[b_\mu(h-h')].$$

At $E\ll a_\mu/b_\mu\approx0.57$ TeV, the radiative and photonuclear energy loss is inessential and thus

$$W_\mu(E,h,h',\vartheta)\simeq\left[\left(\frac{h'}{h}\right)\left(\frac{E}{E+a_\mu(h-h')}\right)\right]^{E_\mu^{cr}(\vartheta)/(E+a_\mu h)}.$$

The combined results of our calculations for the vertical momentum spectrum of conventional muons at sea level can be summarized (with a 2% accuracy) by the following fitting formula:

$$\mathcal{D}_\mu(p,h=1030\text{ g/cm}^2,\vartheta=0°)$$

$$=Cp^{-(\gamma_0+\gamma_1\log p+\gamma_2\log^2 p+\gamma_3\log^3 p)}, \tag{3.4}$$

with parameters presented in Table II for a few momentum ranges [here p is the muon momentum in GeV/c and $\mathcal{D}_\mu(p,h,\vartheta)=(p/E)\mathcal{D}_\mu(E,h,\vartheta)$].

Figure 1 compares our result for the vertical differential muon spectrum at sea level with the results of Volkova *et al.* [78], Dar [79], Butkevich *et al.* [80], Lipari [81], and Agrawal *et al.* [82]. In this comparison, we used the fitting formulas from Refs. [78,79], and the corresponding tables from Refs. [80–82]. In Table III, we show the ratio of each calculated spectrum from Refs. [78–82] to ours for $E=1,10,\ldots,10^6$ GeV. The ratios are inside the wide range 0.75–1.48. In the momentum region from ~5 to 5×10^3 GeV/c, our result is in very good agreement with the recent Monte Carlo calculation by Agrawal *et al.* [82]: the discrepancy is less than 6%. This is consistent with the uncertainties of both calculations caused by the uncertainties in the input
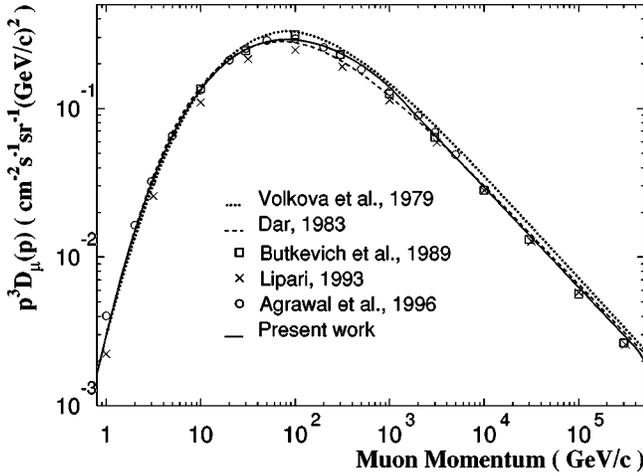
FIG. 1. Vertical differential momentum spectra of conventional muons at sea level calculated by Volkova *et al.* [78], Dar [79], Butkevich *et al.* [80], Lipari [81], Agrawal *et al.* [82], and in the present work.

parameters. At low energies (1–10 GeV), our calculation agrees closely with the fitting formulas by Volkova *et al.* [78] and Dar [79].

IV. CHARM PRODUCTION AND PROMPT MUONS

The prompt muon and neutrino component of the cosmic-ray flux originates from the decay of short-lived particles (mainly charmed hadrons $D^{\pm}$, D^0, $\bar{D}^0$, Λ_c^+, . . .) produced in interactions of cosmic rays with the atmosphere. For the last 15 years, a lot of papers with calculations of prompt lepton production in the atmosphere have been published with very different outputs. Suffice it to say that the predicted energy at which the vertical sea-level PM flux becomes equal to that of muons from π and K decays varies from ~ 20 TeV to $\sim 10^3$ TeV, depending on the adopted charm production model. Early works [83–90] were based on empirical *ad hoc* models for open-charm production and some extrapolations of the accessible (rather fragmentary) accelerator data to the orders-of-magnitude higher energies of the primary and secondary particles participant in cosmic-ray interactions. The successive works apply more advanced phenomenological approaches to the charm-production problem [3,5,91–94] or a set of parametrizations for the energy dependence of the inclusive cross sections which qualita-

TABLE III. The ratios of vertical differential spectra of conventional muons calculated by different workers to ours.

Ref.	E (GeV)						
	1	10	10^2	10^3	10^4	10^5	10^6
[78]	1.010	0.996	1.135	1.056	1.189	1.156	1.483
[79]	1.001	1.046	0.958	0.873	1.023	1.047	1.405
[80]	–	1.015	1.079	0.909	0.958	0.902	1.140
[81]	0.753	0.820	0.858	0.823	0.955	0.923	1.160
[82]	1.355	0.992	1.017	0.938	–	–	–

tively describe the main features of some popular models for charm production [4,95]. Let us briefly look at two recent approaches based on the perturbative QCD (PQCD) and the dual parton model (DPM) [5,94].

Thunman, Ingelman, and Gondolo [5] apply a state-of-the-art model to simulate charm hadroproduction through PQCD processes. To leading order in the coupling constant α_s, these are the gluon-gluon fusion ($gg \rightarrow c\bar{c}$) and the quark-antiquark annihilation ($q\bar{q} \rightarrow c\bar{c}$). The next-to-leading order, $\mathcal{O}(\alpha_s^3)$, contributions are taken into account by doubling the cross sections. To simulate the primary and cascade interactions, the authors use the well-accepted Monte Carlo code PYTHYA. Without going into details of their approach, we emphasize that the PM flux predicted by Thunman *et al.* is one of the lowest ones. It overcomes the vertical π,K-muon flux at energy of about 2×10^3 TeV and therefore is undistinguished in present-day ground-based undeground, and underwater muon experiments.

In the paper by Battistoni *et al.* [94], a new Monte Carlo calculation of the PM fraction in atmospheric showers was made using the DPMJET-II code based on the two-component DPM and interfaced to the shower code HEMAS. The calculation does not yield the absolute PM flux but, from the estimated prompt-to-conventional muon ratio, one can see a leastwise qualitative agreement with the result of Ref. [5]. In particular, according to the DPM, the prompt component overcomes the conventional one in the region of 1–3 PeV (not reachable with the simulated statistics).

In our previous works [3,91,92], the two different phenomenological nonperturbative approaches to the charm-production problem have been applied, the recombination quark-parton model (RQPM) and the quark-gluon string model (QGSM). In the present calculation, we use just these two models. For this reason, the most salient features of them will be outlined below in this section. The RQPM will be discussed at greater length, considering that the QGSM is well accepted and covered adequately in the literature [96] (see also Refs. [1] and [97] for reviews). As an example of a calculation giving a particularly high PM flux, we will also sketch a semiempirical model put forward by Volkova *et al.* [90]. Comprehensive reviews of the current experimental status of the charm-production problem can be found in Ref. [98].

A. Models for charm hadroproduction

1. Recombination quark-parton model

The RQPM is one of the models with ''intrinsic charm.'' The models of this class are based on the following key assumptions.

(i) The projectile wave contains an intrinsic-charm Fock component (see Refs. [99,100]). As an example, Fig. 2 shows the component $|uudc\bar{c}\rangle$ generated by the virtual sub-process $gg \rightarrow c\bar{c}$ where the initial gluons couple to two (or more) valence quarks of the projectile.

(ii) The interaction of partons in the final state leads to a recombination (or coalescence) of the charmed quark with projectile fragments and to production of leading charmed hadrons [101–103].
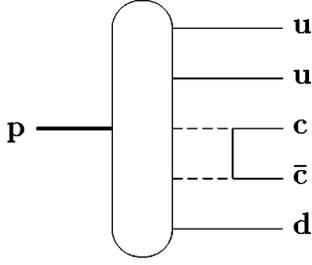
FIG. 2. Intrinsic $|uudc\bar{c}\rangle$ Fock component in the wave function of a projectile proton.

An indication in favor of these models was found in muon-nucleon scattering [104]. It was shown that there exists a visible excess of the charmed particle yield at $x_F \gtrsim 0.15$ and $Q^2 \lesssim 40$ GeV^2 over the model expectations based on photon-gluon fusion and conventional QCD evolution. The upper bound for the probability to find an intrinsic-charm Fock component in the proton wave is about 0.6%.

It has been shown by Brodsky *et al.* [100] that diagrams with intrinsic charm, in which a $c\bar{c}$ pair is coupled to more than one constituent of the projectile hadron, are suppressed by powers of $M_{c\bar{c}}^2(1-x_c)$ (here $M_{c\bar{c}}$ is the invariant mass of the pair and x_c is the fraction of hadron momentum carried by a parton); i.e., the relative contribution of the intrinsic-charm mechanism to the longitudinal momentum distribution of charmed hadrons is expected to be especially large in the fragmentation region of a projectile. In other words, intrinsic-charm models predict relatively hard inclusive spectra. At the same time, the total inclusive cross section can be rather large (it depends strongly on the assumptions about the charm structure function of the projectile hadron). These features cannot be obtained in perturbation theory (see, e.g., Ref. [105] where a comparison of 600 GeV π^- emulsion data with the next-to-leading order PQCD predictions was made).

In the RQPM, the process of hadronization occurs by means of a recombination of quarks to hadrons [102]. It is assumed that only slow ("wee") partons of colliding hadrons take part in the interaction and the distributions of fast partons do not change during the collision. Therefore the inclusive spectra of produced particles (those with small p_T and with not too small x_F) are entirely governed by quark distributions inside the projectile hadron.

a. Charm production in hadron-nucleon collisions. The inclusive cross section for production of a meson $M = q\bar{q}$ in pp interaction is

$$x_F \frac{d\sigma_{pp \to MX}}{dx_F} = \sum_{ij} \int \sigma_{ij}(x_{q_i}, x_{q_j}) F_{p_1}^{(1)}(x_{q_i}) F_{p_2}^{(3)}(x_{q_j}, x_q, x_{\bar{q}})$$

$$\times R_M(x_q, x_{\bar{q}}; x_F) dx_{q_i} dx_{q_j} dx_q dx_{\bar{q}}. \quad (4.1)$$

Here q_i and q_j are the "wee" partons from protons p_1 and p_2, respectively (p_2 is the projectile), σ_{ij} is the total cross section for the $q_i q_j$ interaction, $F_{p_k}^{(m)}$ is the m-parton joint distribution inside the proton p_k, and R_M is the function of recombination of the pair $q\bar{q}$ into meson M. The cross sec-

tion (4.1) is written for the *fragmentation region* of the projectile p_2. Let us assume that the distribution of "wee" partons is universal and does not correlate with the distribution of fast partons. Then

$$F_{p_2}^{(3)}(x_{q_j}, x_q, x_{\bar{q}}) = F_{p_2}^{(1)}(x_{q_j}) F_{p_2}^{(2)}(x_q, x_{\bar{q}}).$$

Considering that

$$\sigma_{pp}^{tot} = \sum_{ij} \int \sigma_{ij}(x_{q_i}, x_{q_j}) F_{p_1}^{(1)}(x_{q_i}) F_{p_2}^{(1)}(x_{q_j}) dx_{q_i} dx_{q_j}$$

yields

$$x_F \frac{d\sigma_{pp \to MX}}{dx_F} = \sigma_{pp}^{tot} \int F_p^{(2)}(x_q, x_{\bar{q}}) R_M(x_q, x_{\bar{q}}; x_F) dx_q dx_{\bar{q}}.$$

In a similar spirit one can derive the inclusive cross section for the generic reaction $iN \to fX$:

$$x_F \frac{d\sigma_{iN \to fX}}{dx_F} = \sigma_{iN}^{tot}(s) \int F_i(\{x_k\}) R_f(\{x_k\}; x_F) \prod_k dx_k. \quad (4.2)$$

Here x_k is the fraction of the projectile momentum which belongs to the parton q_k, $F_i(\{x_k\})$ is the two- or three-quark distribution in the projectile hadron i, and $R_f(\{x_k\}; x_F)$ is the function of recombination of two or three quarks into hadrons.

It would appear reasonable that far away from the threshold of open-charm production, the parton distributions and recombination functions do not depend on the projectile particle energy. Then the s dependence of the $d\sigma_{iN \to fX}/dx_F$ is determined by the energy dependence of the total cross section for the iN interaction, $\sigma_{iN}^{tot}(s)$, and therefore the scaling violation is fairly small. As in the case of light-particle production, we use for the $\sigma_{iN}^{tot}(s)$ the model of elastic amplitude from Ref. [72] which predicts that the total cross section grows as $\ln s$ at the asymptotic energies.

We assume that the c-quark sea in a hadron is essentially nonperturbative and it is characterized by a flat momentum spectrum (see, e.g., Ref. [99]). According to the parton conception, in the infinite momentum frame, the lifetime of fluctuations containing heavy quarks is very large; the flatness of heavy-quark spectra follows from a simple picture of a hadron as an aggregate of partons with approximately equal velocities and from calculations of structure functions for strongly coupled states.

To calculate the two- and three-quark distributions $F_i(\{x_k\})$, we use the statistical approach by Kuti and Weisskopf [106]. The functions $F_i(\{x_k\})$ are constructed through "uncorrelated" parton distributions $f_k^{val}(x)$ and $f_k^{sea}(x)$ for valence and sea quarks ($k = u, d, s, c$) and through the correlation functions $G^i(1-x)$. For example, the two-particle distribution of u and $\bar{c}$ quarks in a proton is of the form

$$F_p^{(2)}(x_u,x_{\bar{c}})=[2G_u^p(1-x_u-x_{\bar{c}})f_u^{\mathrm{val}}(x_u)$$
$$+G_0^p(1-x_u-x_{\bar{c}})f_u^{\mathrm{sea}}(x_u)]f_c^{\mathrm{sea}}(x_{\bar{c}}).$$

The three-particle distribution of u, d, and c in a proton is

$$F_p^{(3)}(x_u,x_d,x_c)=\left[2G_{ud}^p\left(1-\sum x_q\right)f_u^{\mathrm{val}}(x_u)\right.$$
$$+G_d^p\left(1-\sum x_q\right)f_u^{\mathrm{sea}}(x_u)\right]f_d^{\mathrm{val}}(x_d)f_c^{\mathrm{sea}}(x_c)$$
$$+\left[2G_u^p\left(1-\sum x_q\right)f_u^{\mathrm{val}}(x_u)\right.$$
$$+G_0^p\left(1-\sum x_q\right)f_u^{\mathrm{sea}}(x_u)\right]f_d^{\mathrm{sea}}(x_d)f_c^{\mathrm{sea}}(x_c),$$

$$\sum x_q=x_u+x_d+x_c.$$

Both the uncorrelated distributions and correlation functions for light quarks and gluons in a proton and pion were calculated by Takasugi and Tata [107] in the framework of the statistical model using all appropriate accelerator data. It can be shown that the correlation functions are little affected by introducing the sea of charmed quarks and hence we will use the results of Ref. [107] without any modifications. In so doing and using Eq. (4.2), the uncorrelated c distributions $f_c^{\mathrm{sea}}(x)$ could be basically extracted from the data on charm production. In fact the realization of this program is somewhat limited because Eq. (4.2) only holds at asymptotic energies (far away from the charm-production threshold) and, besides, the available accelerator data at high energies cover a narrow range $0.1 \lesssim x_F \lesssim 0.9$. Within this range, the best fit of the ISR data on Λ_c production in pp interactions [108] and the European Muon Collaboration (EMC) data on charm production in deep-inelastic muon scattering [104] is achieved with the following simple parametrizations [102]:

$$f_c^{\mathrm{sea}}(x)=\begin{cases}5.5\times10^{-3}x^{-0.5}(1-x)^{-1.83} & \text{for protons,}\\7.7\times10^{-3}x^{-1}(1-x)^{-0.85} & \text{for pions.}\end{cases}$$

In our calculations, we do not make distinctions between pseudoscalar and vector charmed mesons of an identical quark composition at production. So by a D meson production cross section is meant the overall cross section for the production of D and D^* mesons.

For the recombination functions of quarks into D and Λ_c we use the formulas derived by Hwa in his valon model [109]:

$$R_D(x_1,x_2;x)=\frac{x}{B(a,b)}\left(\frac{x_1}{x}\right)^a\left(\frac{x_2}{x}\right)^b\delta(x_1+x_2-x),$$

$$R_{\Lambda_c}(x_1,x_2,x_3;x)=\frac{x}{B(a,b)B(a,a+b)}\left(\frac{x_1x_2}{x}\right)^a\left(\frac{x_3}{x}\right)^b$$
$$\times\delta(x_1+x_2+x_3-x).$$

Here $B(a,b)$ is the beta function, and a and b are constants defined by the form of the valon distributions. Regarding the valons as constituent quarks bound nonrelativistically in a bag, it can be shown [109] that their average momenta $\langle x_i\rangle$ are proportional to their masses $\hat{m}_i$. Then, considering the two-valon distribution in a D^0 meson, we have

$$\frac{a}{b}=\frac{\langle x_u\rangle}{\langle x_{\bar{c}}\rangle}=\frac{\hat{m}_u}{\hat{m}_c}\simeq\frac{1}{6}.$$

Below, we adopt $a=1$ in all numerical calculations.

b. Nuclear effects. In order to take nuclear effects into account, we use the additive quark model [110]. Let us assume that passing over the target nucleus A a valence quark of the projectile behaves as a free particle between its collisions with nuclei. If at a collision with a nucleus the quark loses the bulk of its momentum, that quark may be thought of as captured by the target and its contribution to the production (through the recombination) of hadrons with large x_F can be neglected. On the contrary, the quark which escapes collisions can hadronize by recombining with slow quark(s) as described above. Because our prime interest is in the high-energy range and in the fragmentation region of projectile particles, one can neglect the interaction of secondary hadrons with the target nucleus. Indeed, the time of generation of hadrons is proportional to their momenta and fast hadrons are produced outside the nucleus. In line with these assumptions, the invariant cross section for inclusive production of hadrons in hadron-nucleus collisions is expressed in terms of the ''recombination'' hadron-nucleus cross sections and the probabilities for capturing valence quarks by the target nucleus. Using standard ''nuclear optics'' techniques [111] and the additive-quark-model relations for the total cross sections [110], $2\sigma_{pp}\simeq3\sigma_{\pi p}\simeq2\sigma_{qp}$ ($q=u,\bar{u},d,\bar{d}$), one can derive the following formulas for the inclusive charm-production cross sections [102]:

$$\frac{d\sigma_{pA\to D^+X}}{dx_F}=3\left(\frac{\sigma_{\pi A}-\sigma_{qA}}{\sigma_{pp}}\right)\frac{d\sigma_{pp\to D^+X}}{dx_F},$$

$$\frac{d\sigma_{pA\to D^-X}}{dx_F}=3\left(\frac{\sigma_{pA}-\sigma_{qA}}{\sigma_{pp}}\right)\frac{d\sigma_{pp\to D^-X}^{[d_v\bar{c}]}}{dx_F}$$
$$+3\left(\frac{\sigma_{\pi A}-\sigma_{qA}}{\sigma_{pp}}\right)\frac{d\sigma_{pp\to D^-X}^{[d_s\bar{c}]}}{dx_F},$$

$$\frac{d\sigma_{pA\to D^0X}}{dx_F}=3\left(\frac{\sigma_{\pi A}-\sigma_{qA}}{\sigma_{pp}}\right)\frac{d\sigma_{pp\to D^0X}}{dx_F},$$

$$\frac{d\sigma_{pA\to\bar{D}^0X}}{dx_F}=\left(\frac{\sigma_{pA}+\sigma_{\pi A}-2\sigma_{qA}}{\sigma_{pp}}\right)\frac{d\sigma_{pp\to\bar{D}^0X}^{[u_v\bar{c}]}}{dx_F}$$
$$+3\left(\frac{\sigma_{\pi A}-\sigma_{qA}}{\sigma_{pp}}\right)\frac{d\sigma_{pp\to\bar{D}^0X}^{[u_s\bar{c}]}}{dx_F},$$

$$\frac{d\sigma_{pA\to\Lambda_c^+X}}{dx_F}=3\left(\frac{\sigma_{pA}-\sigma_{\pi A}}{\sigma_{pp}}\right)\frac{d\sigma_{pp\to\Lambda_c^+X}^{[u_vd_vc]}}{dx_F}$$

$$+\left(\frac{\sigma_{pA}+\sigma_{\pi A}-2\sigma_{qA}}{\sigma_{pp}}\right)\frac{d\sigma_{pp\to\Lambda_c^+X}^{[u_vd_sc]}}{dx_F}$$

$$+\frac{3}{2}\left(\frac{\sigma_{pA}-\sigma_{qA}}{\sigma_{pp}}\right)\frac{d\sigma_{pp\to\Lambda_c^+X}^{[u_sd_vc]}}{dx_F}$$

$$+3\left(\frac{\sigma_{\pi A}-\sigma_{qA}}{\sigma_{pp}}\right)\frac{d\sigma_{pp\to\Lambda_c^+X}^{[u_sd_sc]}}{dx_F},$$

$$\frac{d\sigma_{\pi^+A\to DX}}{dx_F}=2\left(\frac{\sigma_{\pi A}-\sigma_{qA}}{\sigma_{\pi p}}\right)\frac{d\sigma_{\pi p\to DX}}{dx_F}$$

$$(D=D^\pm,D^0,\bar{D}^0).$$

Here $d\sigma_{ip\to fX}^{[\cdots]}/dx_F$ is the contribution to the iN cross section from a quark diagram with a final hadron f that contains the leading valence (v) or sea (s) quarks indexed in the brackets. To sufficient accuracy, the total cross sections in the foregoing equations are assumed to be energy independent. In our numerical evaluations, we set $\sigma_{iA}=\sigma_{iA}^0$ for the hadron-nucleus cross sections (see Sec. II) and $\sigma_{qp}=13.0$ mb for the quark-proton cross section [111]. The numerical results are represented in the traditional form

$$\frac{d\sigma_{iA\to fX}}{dx_F}=A^{\alpha(x_F)}\frac{d\sigma_{iN\to fX}}{dx_F}.$$

For the reactions $pA\to D^+X$, $pA\to D^0X$, and $\pi A\to DX(D=D^\pm,D^0,\bar{D}^0)$, $\alpha=0.765$, independently of x_F. It should be pointed out that accelerator data at low energies show a higher value of α. For example, in the WA82 experiment [112] (a 340 GeV π^- beam) the value $\alpha=0.92\pm0.06$ was obtained for D mesons with $\langle x_F\rangle=0.24$. However, it seems plausible that this is a reflection of the "near-threshold effect" and the α will decrease with a rise of the projectile energy. In any event, nonperturbative effects should become more important as $\sqrt{s}$ and x_F increase and therefore shadowing is expected to become more essential at higher center-of-mass energies and at large x_F [113].

For the rest reactions and within the range $0.10\le x_F\le0.95$, the functions $\alpha(x_F)$ may be parametrized as follows:

$$\alpha_{pA\to\bar{D}^0X}(x)=0.754-0.034x-0.008x^2+0.020x^3,$$

$$\alpha_{pA\to D^-X}(x)=0.769-0.158x+0.272x^2-0.174x^3,$$

$$\alpha_{pA\to\Lambda_c^+X}(x)=0.780-0.367x+0.672x^2-0.456x^3.$$

TABLE IV. Parameters $Z_{fi}(\gamma,E_\gamma)$ of fitting formula (4.3) for the fractional moments $Z_{fi}(\gamma,E)$ calculated with the RQPM for the two values of γ.

			f		
i	D^+	D^-	D^0	$\bar{D}^0$	Λ_c^+
			$\gamma=1.62$		
p	4.6×10^{-4}	6.5×10^{-4}	3.8×10^{-4}	6.9×10^{-4}	4.9×10^{-4}
π^+	1.3×10^{-3}	9.0×10^{-4}	9.0×10^{-4}	1.3×10^{-3}	6.0×10^{-4}
			$\gamma=2.02$		
p	5.4×10^{-4}	7.9×10^{-4}	4.5×10^{-4}	8.6×10^{-4}	6.2×10^{-4}
π^+	1.8×10^{-3}	1.2×10^{-3}	1.2×10^{-3}	1.8×10^{-3}	7.9×10^{-4}

These results do not contradict the accelerator data even at very low energies, although the data are rather uncertain yet. For example, the BIS-2 experiment [114] (a 37.5–70 GeV neutron beam) gives $\langle\alpha\rangle=0.73\pm0.23$ for $\bar{D}^0$ production.

As discussed above, we assume that the captured quarks take no part in the recombination. This leads to a small underestimation of the cross sections, because some portion of wounded quarks actually will recombine. Let us estimate the upper limit of the α assuming that *all* the valence quarks of the projectile can recombine. This assumption yields

$$\frac{d\sigma_{iA\to fX}}{dx_F}=\left(\frac{\sigma_{iA}}{\sigma_{iN}}\right)\frac{d\sigma_{iN\to fX}}{dx_F}$$

and thus $\alpha\le0.85$ for $\pi A\to DX$ and $\alpha\le0.79$ for $pA\to D(\Lambda_c)X$. This estimate demonstrates that the uncertainty in the A dependence within our simplified approach does not exceed $\sim15\%$ for the air nuclei.

c. Z factors. Owing to the mentioned small scaling violation, the fractional moments Z_{fi} calculated with the RQPM from Eq. (2.5) are energy dependent. They can be approximated with an accuracy of (2–3)% by the following expression:

$$Z_{fi}(\gamma,E)=Z_{fi}(\gamma,E_\gamma)\left(\frac{E}{E_\gamma}\right)^{\xi_\gamma},\tag{4.3}$$

where E is the energy of secondary particle $f(f=D^\pm,D^0,\bar{D}^0,\Lambda_c^+)$, and E_γ and ξ_γ are the constants dependent on the primary cosmic-ray spectrum. In particular,

$$E_\gamma=10^3\text{ GeV},\quad\xi_\gamma=0.096\quad\text{for }\gamma=1.62,$$

$$E_\gamma=10^6\text{ GeV},\quad\xi_\gamma=0.076\quad\text{for }\gamma=2.02.$$

Parameters $Z_{fi}(\gamma,E_\gamma)$ for $i=p,\pi^+$ are presented in Table IV. For $i=n,\pi^-$ one can use the relations

$$Z_{D^+n}=Z_{D^0p},\quad Z_{D^-n}=Z_{\bar{D}^0p},\quad Z_{D^0n}=Z_{D^+p},$$
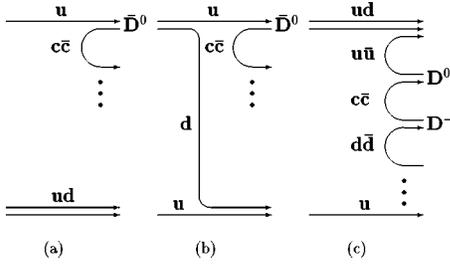
FIG. 3. Fragmentation of quark chains into D mesons in the QGSM: (a),(b) favored fragmentation into $\bar{D}^0$; (c) unfavored fragmentation into D^- and D^0.

$$Z_{\bar{D}^0 n} = Z_{D^- p}, \quad Z_{\Lambda_c^+ n} = Z_{\Lambda_c^+ p}, \quad Z_{D^+ \pi^-} = Z_{\bar{D}^0 \pi^-} = Z_{D^0 \pi^+},$$

$$Z_{D^- \pi^-} = Z_{D^0 \pi^-} = Z_{\bar{D}^0 \pi^+}, \quad Z_{\Lambda_c^+ \pi^-} = Z_{\Lambda_c^+ \pi^+},$$

which follow from considerations of the isotopic symmetry.

2. Quark-gluon string model

The QGSM [96] is a nonperturbative approach to the description of hadron collisions. It is based on the topological $1/N_f$ expansion of QCD diagrams for elastic scattering [115] (associated with the multiple Pomeron exchange expansion) and the string model of hadrons and hadronic interactions. The particles are produced in this model by breaking the strings connecting the incident hadron's constituents (quarks and diquarks).

The QGSM is considered to be one of the most satisfactory of the tools available to represent open-charm production. It describes a great body of data on hadronic interactions at all available energies. However, the model is not free from difficulties. For instance, the QGSM predicts clear-cut flavor correlations. In particular, there must be preferential production of $\bar{D}^0$ mesons in pp collisions ("favored fragmentation") owing to the $(u-ud)$ composition of the proton and $(\bar{c}u)$ composition of $\bar{D}^0$ (Fig. 3). This prediction is not supported by experiment [116], although this disagreement can be caused in part by bad flavor identification in the experiment (see Ref. [1] for a discussion).

To calculate the inclusive cross sections one must know the distribution functions of the dressed quarks (constituents) of the colliding hadrons and the fragmentation functions of these constituents into charmed particles. These functions can be approximately determined by the use of Regge-model arguments [117], in terms of intercepts $\alpha_R \sim -\alpha_N \sim 0.5$, of known Regge poles, and the intercept of the $c\bar{c}$ Regge trajectory, α_ψ, on which there is no direct experimental information. Hence α_ψ is a free parameter of the model. It governs, in particular, the steepness of the inclusive spectra of charmed particles. If the $c\bar{c}$ trajectories are linear (as it is in the case of light quarks and generally in the string models of hadrons), the intercept of the ψ trajectory is fairly large ($\simeq -2.2$) and the longitudinal momentum distributions of charmed hadrons are rather steep. A complete list of the distribution and fragmentation functions as well as the values of their various parameters is given in Ref. [96].

TABLE V. Parameters $Z_{fi}(\gamma, E_\gamma)$ and ξ_γ (in parentheses) of fitting formula (4.3) for the fractional moments $Z_{fi}(\gamma, E)$ calculated with the QGSM for $\gamma = 2.02$ at $E \gtrsim 10^3$ TeV.

			f		
i	D^+	D^-	D^0	$\bar{D}^0$	Λ_c^+
p	6.5×10^{-5}	9.9×10^{-5}	7.1×10^{-5}	2.1×10^{-4}	9.5×10^{-4}
	(0.050)	(0.046)	(0.050)	(0.044)	(0.041)
n	7.1×10^{-5}	1.9×10^{-4}	6.5×10^{-5}	1.2×10^{-4}	9.5×10^{-4}
	(0.050)	(0.045)	(0.050)	(0.045)	(0.041)
π^+	5.5×10^{-4}	1.4×10^{-4}	1.4×10^{-4}	5.5×10^{-4}	1.5×10^{-5}
	(0.041)	(0.048)	(0.048)	(0.041)	(0.035)
π^-	1.4×10^{-4}	5.5×10^{-4}	5.5×10^{-4}	1.4×10^{-4}	1.5×10^{-5}
	(0.048)	(0.041)	(0.041)	(0.048)	(0.035)

Our calculations of the inclusive cross sections within the framework of the QGSM have been done without attempts to optimize the set of parameters of the model. In particular, we do not include the intrinsic charm component as was suggested recently [97]. Below, we are dealing with a qualitative analysis of the QGSM prediction for charm production at cosmic-ray energies rather than with a close examination of the model. For this reason, in evaluating the nuclear effect within the QGSM, we adopt $\alpha = 0.72$ for all processes under consideration. This simplification can lead to a small ($<15\%$) error in the Z factors, compared to the exact calculation within the additive quark model. The energy dependence of the factors $Z_{fi}(\gamma, E)$ calculated with the QGSM is somewhat different as compared with the RQPM prediction. The parametrization (4.3) is valid for the QGSM only at very high energies ($\gtrsim 10^3$ TeV) and the parameters ξ_γ are in general different for different reactions $iA \to fX$. The parameters $Z_{fi}(\gamma, E_\gamma)$ and ξ_γ for $i = p$, n, π^+, and π^- are presented in Table V at $\gamma = 2.02$ (above the knee energy region). The energy dependence of the Z factors at $E < 10^3$ TeV can be found in Ref. [3].

3. Semiempirical model

The model of Volkova, Fulgione, Galeotti, and Scavedra [90] (VFGS) is a typical example of an approach which proceeds from a parametrization of available accelerator data for inclusive spectra of charmed particles together with some additional assumptions to extrapolate the parametrization to the kinematic regions, where data on the inclusive charm production cross sections are absent.

Volkova *et al.* make use of a very steep inclusive spectrum of produced D mesons [$\propto (1-x_D)^5/x_D$, where x_D is the ratio of the D-meson energy to the nucleon energy in the laboratory frame] with a sharp cutoff in the central region ($d\sigma/dx_D = 0$ at $x_D \lesssim 0.05$). In spite of such a cutoff the integral $\int (d\sigma/dx_D) dx_D$ was normalized to the total $D\bar{D}$ cross section $\sigma_{pp}^{D\bar{D}}(E_N)$. Considering the accelerator data at $E_N \gtrsim 1$ TeV together with some implications of the QGSM, it has been adopted that

$$\sigma_{pp}^{D\bar{D}}(E_N) = \begin{cases} 0.48(\log E_N - 3.075) \text{ mb} \quad \text{for } 1 \text{ TeV} \leqslant E_N < 500 \text{ TeV,} \\ 1.26 \text{ mb} \quad \text{for } E_N \geqslant 500 \text{ TeV.} \end{cases}$$

A consequence of this assumption is a relatively strong scaling violation in the fragmentation region.

The VFGS model predicts comparatively large PM flux (see below) since, owing to the cutoff, all produced particles are in the fragmentation region of a projectile (i.e., there is no central part of the inclusive spectrum). It was also assumed that (independently of x_F) $\alpha = 1$ and 2/3 for reactions with D mesons and Λ_c^+ hyperons in the final state, respectively.

The approach of Ref. [90] includes some other assumptions which also tend to increase the PM fraction in comparison with our result. The most important ones are concerned with the primary spectrum, semileptonic decays of charmed particles, and certain elements of the nuclear-cascade model. A more detailed comparison of the approach under consideration against the RQPM and the QGSM, in connection with the PM problem, has been done in Ref. [92].

B. Prompt-muon flux at sea level

1. Interactions and decay of charmed particles

Inasmuch as we neglect the production of nucleons, pions, and kaons by charmed particles and charm regeneration, the transport equations for D and Λ_c spectra are identical in form to Eq. (2.7) for kaons. Notice that the PM flux weakly depends on the specific values of the inelastic cross sections for D and Λ_c up to about 10^4 TeV of muon energy, due to the very short lifetimes of these particles. Thus a rough estimation of $\sigma_{DA}^{\text{inel}}$ and $\sigma_{\Lambda_c^{\pm}A}^{\text{inel}}$ will suffice for our purposes. We use the same formula (2.4) as for the light hadrons with $\sigma_{DA}^0 = 100$ mb ($D = D^{\pm}, D^0, \bar{D}^0$) and $\sigma_{\Lambda_c^{\pm}A}^0 = 200$ mb.

Calculation of the PM flux can be performed in almost perfect analogy to the conventional muon flux with only one essential difference: the PM generation function includes a rich variety of multiparticle semileptonic decay modes. Thus the inclusive approach is best suited to the problem. The corresponding muon generation function may be written as

$$G_\mu^{D,\Lambda_c}(E,h,\vartheta) = \sum_{i=D^{\pm},D^0,\bar{D}^0,\Lambda_c} B(i \to \mu\nu X)$$
$$\times \frac{E_i^{\text{cr}}(\vartheta)}{hE} \int_{x_i^-}^{x_i^+} F_i^\mu(x) \mathcal{D}_i\left(\frac{E}{x},h,\vartheta\right) dx.$$

(4.4)

Here $F_i^\mu(x)$ is the normalized spectrum of muons in the inclusive decay $i \to \mu\nu_\mu X$ ($x = E/E_i$) and

$$x_i^\mp = 2m_\mu^2[(m_i^2 + m_\mu^2 - s_X) \pm \sqrt{(m_i^2 + m_\mu^2 - s_X)^2 - 4m_\mu^2 m_i^2}]^{-1},$$

with s_X the minimal invariant mass square for the hadron system X. The other designations are completely similar to the ones previously used.

To simplify matters we consider the inclusive decay $i \to \mu\nu X$ as a three-particle one. We assume the simplest form of matrix elements according to Ref. [118]. The form factors involved (one for $D \to \mu\nu_\mu X$ and three for $\Lambda_c \to \mu\nu_\mu X$) are replaced with their averaged values. In so doing the mass square of the ''X particle,'' s_X^{eff}, may be fitted in such a way as to correlate the calculated and experimental values for the differential and total decay rates. Omitting rather tedious details of the calculation, we present the final formulas for the muon spectral functions $F_D^\mu(x)$ and $F_{\Lambda_c}^\mu(x)$:

$$F_D^\mu(x) = \frac{1}{Z_D}\left[\frac{1}{6}(1-r_D^2)(1-5r_D^2-2r_D^4) + r_D^4 x - \frac{1}{2}(1-2r_D^2)x^2 + \frac{1}{3}x^3 + r_D^4\ln\left(\frac{1-x}{r_D^2}\right)\right],$$

$$Z_D = \frac{1}{12}(1-r_D^4)(1-8r_D^2+r_D^4) - r_D^4\ln r_D^2,$$

$$F_{\Lambda_c}^\mu(x) = \frac{1}{Z_{\Lambda_c}}\sum_{1\leqslant i\leqslant j\leqslant 3} f_i f_j \mathscr{æ}_{ij}(x), \quad Z_{\Lambda_c} = \sum_{1\leqslant i\leqslant j\leqslant 3} f_i f_j \bar{\mathscr{æ}}_{ij},$$

$$\mathscr{æ}_{11}(x) = \frac{11}{6} - 3r_\Lambda - \frac{21}{2}r_\Lambda^2 - 12r_\Lambda^3 + \frac{9}{2}r_\Lambda^4 + 9r_\Lambda^5 + \frac{7}{6}r_\Lambda^6 + 6r_\Lambda^3(2+r_\Lambda)x - \frac{3}{2}(3-2r_\Lambda-5r_\Lambda^2)x^2 + \frac{8}{3}x^3$$
$$+ \frac{r_\Lambda^4(3+6r_\Lambda+r_\Lambda^2)}{1-x} - \frac{r_\Lambda^6}{(1-x)^2} + r_\Lambda^3(12+9r_\Lambda+6r_\Lambda^2-r_\Lambda^3)\ln\left(\frac{1-x}{r_\Lambda^2}\right),$$

$$\mathscr{e}_{12}(x) = \frac{5}{3} - 6r_\Lambda - 9r_\Lambda^2 - 24r_\Lambda^3 + 3r_\Lambda^4 + 18r_\Lambda^5 - \frac{5}{3}r_\Lambda^6 + 24r_\Lambda^3 x - 3(1 - 2r_\Lambda - r_\Lambda^2)x^2 + \frac{4}{3}x^3$$

$$+ \frac{2r_\Lambda^4(3 + 6r_\Lambda + r_\Lambda^2)}{1-x} - \frac{2r_\Lambda^6}{(1-x)^2} + 2r_\Lambda^3(12 + 3r_\Lambda + 6r_\Lambda^2 - r_\Lambda^3)\ln\left(\frac{1-x}{r_\Lambda^2}\right),$$

$$\mathscr{e}_{13}(x) = -\frac{1}{3} + 3r_\Lambda^2 - 3r_\Lambda^4 - \frac{17}{3}r_\Lambda^6 - 12r_\Lambda^4 x + 3(1 - 3r_\Lambda^2)x^2 - \frac{8}{3}x^3 + \frac{2r_\Lambda^4(3 + r_\Lambda^2)}{1-x} - \frac{2r_\Lambda^6}{(1-x)^2}$$

$$- 2r_\Lambda^4(3 + r_\Lambda^2)\ln\left(\frac{1-x}{r_\Lambda^2}\right),$$

$$\mathscr{e}_{22}(x) = \frac{1}{(1+r_\Lambda)^2}\left[\frac{2}{3} - \frac{4}{3}r_\Lambda - \frac{23}{3}r_\Lambda^2 - 24r_\Lambda^3 - 21r_\Lambda^4 + \frac{40}{3}r_\Lambda^6 + \frac{22}{3}r_\Lambda^7 - \frac{4}{3}r_\Lambda^8 + 2r_\Lambda^3(6 + 9r_\Lambda + 6r_\Lambda^2 - r_\Lambda^3)x\right.$$

$$- \frac{3}{2}(1 - 4r_\Lambda^2 - 4r_\Lambda^3 + r_\Lambda^4)x^2 + \frac{4}{3}(1 + r_\Lambda - r_\Lambda^2)x^3 - \frac{1}{2}x^4 + \frac{r_\Lambda^4(3 + 12r_\Lambda + 14r_\Lambda^2 + 8r_\Lambda^3 + r_\Lambda^4)}{1-x}$$

$$\left. - \frac{r_\Lambda^6(1+r_\Lambda)^2}{(1-x)^2} + r_\Lambda^3(12 + 21r_\Lambda + 24r_\Lambda^2 + 10r_\Lambda^3 + 4r_\Lambda^4 - r_\Lambda^5)\ln\left(\frac{1-x}{r_\Lambda^2}\right)\right],$$

$$\mathscr{e}_{23}(x) = \mathscr{e}_{13}(x),$$

$$\mathscr{e}_{33}(x) = \frac{11}{6} + 3r_\Lambda - \frac{21}{2}r_\Lambda^2 + 12r_\Lambda^3 + \frac{9}{2}r_\Lambda^4 - 9r_\Lambda^5 + \frac{7}{6}r_\Lambda^6 - 6r_\Lambda^3(2 - r_\Lambda)x - \frac{3}{2}(3 + 2r_\Lambda - 5r_\Lambda^2)x^2 + \frac{8}{3}x^3$$

$$+ \frac{r_\Lambda^4(3 - 6r_\Lambda + r_\Lambda^2)}{1-x} - \frac{r_\Lambda^6}{(1-x)^2} - r_\Lambda^3(12 - 9r_\Lambda + 6r_\Lambda^2 + r_\Lambda^3)\ln\left(\frac{1-x}{r_\Lambda^2}\right),$$

$$\bar{\mathscr{e}}_{11} = (1 - r_\Lambda^2)(1 - 2r_\Lambda - 7r_\Lambda^2 - 20r_\Lambda^3 - 7r_\Lambda^4 - 2r_\Lambda^5 + r_\Lambda^6) - 24r_\Lambda^3(1 + r_\Lambda^2 + r_\Lambda^3)\ln r_\Lambda,$$

$$\bar{\mathscr{e}}_{12} = (1 - r_\Lambda^2)(1 - 4r_\Lambda - 7r_\Lambda^2 - 40r_\Lambda^3 - 7r_\Lambda^4 - 4r_\Lambda^5 + r_\Lambda^6) - 24r_\Lambda^3(2 + r_\Lambda + 2r_\Lambda^2)\ln r_\Lambda,$$

$$\bar{\mathscr{e}}_{13} = \bar{\mathscr{e}}_{23} = 0,$$

$$\bar{\mathscr{e}}_{22} = \frac{1}{(1+r_\Lambda)^2}\left[\frac{2}{5} - r_\Lambda - 6r_\Lambda^2 - 28r_\Lambda^3 - 32r_\Lambda^6 + 28r_\Lambda^7 + 6r_\Lambda^8 + r_\Lambda^9 - \frac{2}{5}r_\Lambda^{10}\right.$$

$$\left. - 24r_\Lambda^3(1 + 2r_\Lambda + 3r_\Lambda^2 + 2r_\Lambda^3 + r_\Lambda^4)\ln r_\Lambda\right],$$

$$\bar{\mathscr{e}}_{33} = (1 - r_\Lambda^2)(1 + 2r_\Lambda - 7r_\Lambda^2 + 20r_\Lambda^3 - 7r_\Lambda^4 + 2r_\Lambda^5 + r_\Lambda^6) + 24r_\Lambda^3(1 - r_\Lambda - r_\Lambda^2)\ln r_\Lambda.$$

Here $r_D^2 = s_X^{\text{eff}}/m_D^2$, $r_\Lambda^2 = s_X^{\text{eff}}/m_{\Lambda_c}$, and s_X^{eff} is the effective invariant mass square. The best fit to the data on the differential and total decay rates is achieved using

$$\sqrt{s_X^{\text{eff}}} = \begin{cases} 0.63 \text{ GeV} & \text{for } D^+ \text{ and } D^-, \\ 0.67 \text{ GeV} & \text{for } D^0 \text{ and } \bar{D}^0, \\ 1.27 \text{ GeV} & \text{for } \Lambda_c. \end{cases}$$

Therefore $r_{D^\pm} \approx 0.337$, $r_{D^0, \bar{D}^0} \approx 0.359$, and $r_\Lambda \approx 0.551$. For

the decay form factors averaged over q^2 we have $f_1 \approx 0.991$, $f_2 \approx 2.170$, and $f_3 \approx 0.805$.

2. Parametrization of the calculated PM flux

In the energy region $5 \text{ TeV} \lesssim E \lesssim 5 \times 10^3 \text{ TeV}$ the differential spectra of PM in the vertical direction at sea level, $\mathcal{D}_\mu^{\text{pr}}(E)$, calculated in Ref. [3] with the RQPM and the QGSM, can be approximated by

$$\mathcal{D}_\mu^{\text{pr}}(E, h = 1030 \text{ g/cm}^2, \vartheta = 0°)$$

$$= C'\left(\frac{E_b}{E}\right)^{\gamma'}\left[1 + \left(\frac{E_b}{E}\right)^{\gamma' - 1}\right]^{-a}. \tag{4.5}$$

Here

$$C' = 4.53 \times 10^{-18} \text{ cm}^{-2} \text{ s}^{-1} \text{ sr}^{-1} \text{ GeV}^{-1}, \qquad \gamma' = 2.96,$$

$$a = 0.152 \quad (\text{RQPM}),$$

$$C' = 1.09 \times 10^{-18} \text{ cm}^{-2} \text{ s}^{-1} \text{ sr}^{-1} \text{ GeV}^{-1}, \qquad \gamma' = 3.02,$$

$$a = 0.165 \quad (\text{QGSM}),$$

and $E_b = 10^5$ GeV in both cases. Equation (4.5) fits the numerical results with accuracy better than 4%. With the same accuracy it is also valid for zenith angles $\vartheta \lesssim 80°$ in the energy interval $10-10^3$ TeV, i.e., within the ''region of isotropy'' of the PM flux (see Ref. [3] for more details). Beyond the interval $5-5 \times 10^3$ TeV, Eq. (4.5) can be used as an extrapolation of our result which would suffice for calculating the muon DIR. From Eq. (4.5) we find the following expression for the integral PM spectrum:

$$\mathcal{I}_\mu^{\text{pr}}(E, h = 1030 \text{ g/cm}^2, \vartheta = 0°)$$

$$= \frac{C' E_b}{(\gamma' - 1)(1 - a)}\left\{\left[1 + \left(\frac{E_b}{E}\right)^{\gamma' - 1}\right]^{1 - a} - 1\right\}.$$

A comparison of our calculation of the PM flux with the results of other authors can be found in Refs. [3,91,92] (see also [95]).

According to Ref. [37], the differential and integral PM spectra calculated in the VFGS model can be approximated (at all zenith angles) by

$$\mathcal{D}_\mu^{\text{pr}}(E, h = 1030 \text{ g/cm}^2, \vartheta)$$

$$= 2.92 \times 10^{-5} E^{-2.48} \text{ cm}^{-2} \text{ s}^{-1} \text{ sr}^{-1} \text{ GeV}^{-1},$$

$$\mathcal{I}_\mu^{\text{pr}}(E, h = 1030 \text{ g/cm}^2, \vartheta)$$

$$= 1.97 \times 10^{-5} E^{-1.48} \text{ cm}^{-2} \text{ s}^{-1} \text{ sr}^{-1}$$

(E in GeV). This approximation holds true to about 10^3 TeV.

V. CALCULATED SEA-LEVEL MUON SPECTRA vs EXPERIMENT

Comparison of the calculated differential and integral muon spectra with direct data from spectrometers and indirect data extracted from underground measurements is shown in Figs. 4(a),4(b) and 5(a),5(b). The ground-based measurements can be classified as absolute and nonabsolute (normalized). In line with this arrangement we present here the following three groups of experiments.

Absolute ground-based measurements with MARS apparatus in Durham (Aurela and Wolfendale [7], Ayre *et al.* [12]); Nottingham spectrograph (Baber *et al.* [8], Rastin [14]); spectrometer near College Station, Texas (Bateman
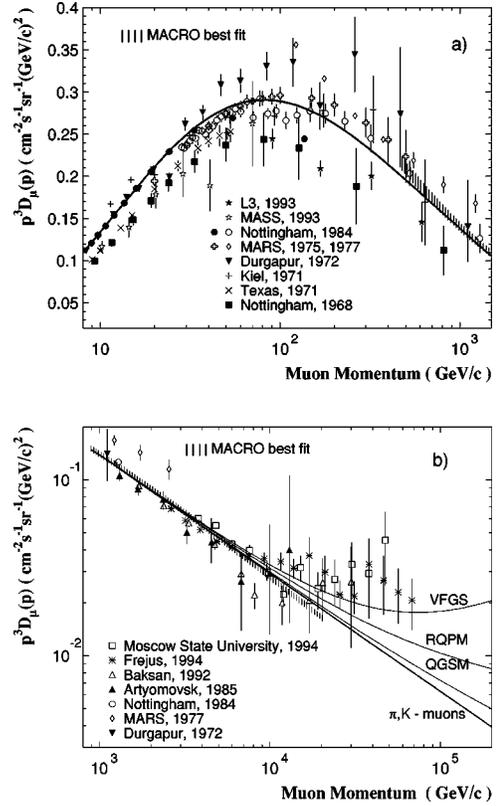
FIG. 4. Vertical differential momentum spectrum of muons at sea level. The direct data are taken from Refs. [8–16], and indirect (underground) data are from Refs. [44,60,62–64]. The shaded areas are for the MACRO fit [44]. The solid curves represent the results of this work for the conventional (π,K) differential muon spectrum and for the π,K muon spectrum plus the PM contribution calculated according to the QGSM, RQPM, and VFGS model.

et al. [9]); Kiel spectrographs (Allkofer *et al.* [10]), MASS apparatus at Prince Albert, Saskatchewan (De Pascale *et al.* [15]); EAS-TOP array at Campo Imperatore, Gran Sasso (Aglietta *et al.* [17]).

Nonabsolute ground-based measurements with Durgapur spectrograph (Nandi and Sinha [11], the data were normalized to the Nottingham spectrum [14] at $p = 20$ GeV/c); Durham spectrograph MARS (Thompson *et al.* [13]; the data were normalized to the previous MARS results [12] at 261 GeV/c); L3 detector at CERN (Bruscoli and Pieri [16]; the absolute intensity in the momentum range 40–70 GeV/c and its error were taken from the Kiel result [10]).

Indirect data from several detectors in the Kolar Gold Fields (Ito [38], Miyake *et al.* [58], Adarkar *et al.* [61]); unimodular scintillation detector ''Collapse'' of the Institute for Nuclear Research (INR) at the Artyomovsk Scientific Station (Khalchukov *et al.* [60]); Baksan underground scintillation telescope of INR situated in North Caucasus (Andreyev *et al.* [36,37], Bakatanov *et al.* [62]); x-ray emulsion chambers of Moscow State University situated in the Moscow metro (Zatsepin *et al.* [64]); proton decay detector Fréjus under the Alps (Rhode [63]); detector MACRO at the Gran Sasso National Laboratory (Ambrosio *et al.* [44]).

The marked curves in Figs. 4 and 5 refer to the differen-
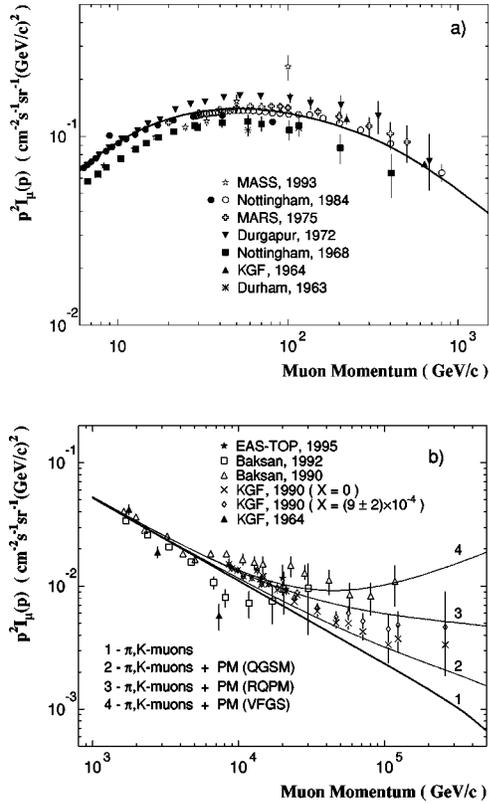
FIG. 5. Vertical integral momentum spectrum of muons at sea level. The direct data are taken from Refs. [7,8,11,12,14,15,17], and indirect (underground) data are from Refs. [37,38,58,62]. The solid curves represent the results of this work for the conventional (π,K) integral muon spectrum and for the π,K muon spectrum plus the PM contribution calculated according to the QGSM, RQPM, and VFGS model.

tial and integral muon spectra, respectively, calculated without the PM contribution (''π,K'' muons) and with the PM contribution according to the three charm production models (QGSM, RQPM, and VFGS) under consideration. As seen from the figures, the PM contribution to the sea-level muon flux calculated with the QGSM is very small: up to $p=100$ TeV/c it does not exceed 16% for the differential spectrum and 22% for the integral spectrum.

Unfortunately, it is difficult to extract some quantitative assessment for the validity of our nuclear-cascade model from the presented set of data even at $p\lesssim1$ TeV/c. As is seen from Figs. 4(a) and 5(a), a wide disagreement between the results of different experiments takes place despite the fact that the quoted errors are relatively small in the majority of the experiments. It indicates the existence of significant systematic errors in some experiments which may be as much as (30–35)% at momenta 10–1000 GeV/c.

It should be noted in this connection that only statistical errors are indicated in the data points of the MASS experiment. According to Ref. [15], the systematic errors in the MASS experiment may be as much as 15% at $p\gtrsim40$ GeV/c. The systematics in the nonabsolute measurements is, as a general rule, unknown. For example, no attempt was made to estimate the systematic errors in the CERN L3 experiment

[16]. In our opinion, the L3 spectrum was underestimated owing to incompletely correct normalization.

At $p\lesssim2$ TeV/c our prediction, regardless of the charm-production model, is in very good agreement with the Nottingham direct and absolute measurements [14].

At energies above a few TeV we only have indirect data at our disposal [119] and the uncertainties (both statistical and systematic) are vastly greater here. The data of Refs. [37,38,44,58,61,63] have been deduced from the muon DIR measured in different rocks (Baksan, Kolar, Alpine, Gran Sasso). We will dwell on the initial underground data in Sec. VII. Here, it should be pointed out that in all underground experiments, among the systematic uncertainties related to inhomogeneities in density and chemical composition of the matter overburden, topographical map resolution, muon range-energy relation, muon range fluctuations, effective differential aperture of the array, etc., another uncertainty is essential. It results from the necessity to assign some model for the energy spectrum and zenith-angle distribution of muons at sea level which are functions of the PM fraction in the muon flux or, to be more specific, the ratio X of the prompt-muon spectrum to the $\pi+K$ production one. Hence one is forced to assume some value of the ratio X (as a function of energy) when reconstructing the sea-level vertical muon spectrum. But the greater the adopted value of X, the harder the resultant spectrum. For this reason alone the conversion procedure is fairly ambiguous.

As an illustration we consider the KGF results. The KGF muon spectrum in the energy range 200–7500 GeV was deduced [58] using the underground data from Ref. [26] and assuming $X=0$, which is quite reasonable for this range. But the data at higher energies [38] (see also Ref. [61]) demand a nonzero X. To estimate the ratio X, the authors have assumed a pion-production spectrum of the form $F(E_\pi)\propto E_\pi^{-\gamma}$ and a K/π ratio of 0.15. The X ratio was assumed to be a constant. Then a χ^2 analysis indicated that with $\gamma=2.7$ for muon energy of 8–250 TeV, there is PM production at the level of $X=(9\pm2)\times10^{-4}$. In Fig. 5(b), we show this result (the corresponding data points are represented by diamonds) together with the spectrum deduced on the assumption that $X=0$ (the data points are represented by the symbol $\times$). As would be expected, the spectrum reconstructed with $X=0$ is softer. It is not difficult to understand that the final result is subject to variation also in response to variation of the adopted K/π ratio and γ [120]. It should also be recognized that the real spectra of muons and mesons are far short of being power-law ones.

Let us touch briefly on some essential points of the rest of the underground data presented in Figs. 4(b) and 5(b).

In the Baksan experiment [37], $X=(1.5\pm0.5)\times10^{-3}$ was found as the best fit of the calculated total intensity of conventional and prompt muons to the experimental data, assuming a power-law primary nucleon flux with spectral index $\gamma_N=1.65$.

In Ref. [63] the complete data set of downgoing muons recorded with the Fréjus detector [39] has been reanalyzed. However, in this analysis, the sea-level spectrum was derived using in essence the continuous loss approximation with some effective and energy-independent energy loss coeffi-

cients. The muon range fluctuations are discussed in Ref. [63] exclusively to estimate the uncertainty of the analysis. But it is a matter of common knowledge that, on calculation of the muon DIR, the continuous loss approximation results in a downward bias and the corresponding error increases fast with depth [121–124]. It is our opinion that the muon spectrum obtained in Ref. [63] was significantly overestimated while the systematic errors were underestimated for $E \gtrsim 10$ TeV in consequence of the oversimplified analysis.

The MACRO fit [44] presented in Figs. 4(a),4(b) by shaded areas has the following form:

$$\mathcal{D}_\mu^{\text{MACRO}}(E, h = 10^3 \ \text{g/cm}^2, \vartheta)$$

$$= C_0 \left(\frac{E}{1 \ \text{GeV}} \right)^{-\gamma_\mu}$$

$$\times \left(\frac{1}{1 + \dfrac{1.1 E \cos \vartheta}{115 \ \text{GeV}}} + \frac{0.054}{1 + \dfrac{1.1 E \cos \vartheta}{850 \ \text{GeV}}} \right), \qquad (5.1)$$

with $C_0 = (0.26 \pm 0.01)$ cm^{-2} s^{-1} sr^{-1} GeV^{-1} and $\gamma_\mu = 2.78 \pm 0.01$. The quoted errors are due to statistics and the topographical map resolution. According to Ref. [44], the overall systematic error resulting from rock density uncertainties and hard energy loss cross sections is about 5% in C_0 and, what is much more important, 3% in γ_μ. But a 3% variation in γ_μ corresponds to uncertainties of 47%, 78%, and more than 100% in the surface muon flux at energies of 10^2, 10^3, and 10^4 GeV, respectively. Therefore, the result of MACRO is greatly uncertain and *pro forma* it is not in contradiction with all the rest of indirect data shown in Fig. 4.

The results of the rest of the underground experiments were obtained with quite different methods. The experiment with the Artyomovsk 100-ton installation ''Collapse'' [60] (situated in a salt mine at the depth of 570 m w.e.) detects the energy release of the showers produced by cosmic-ray muons in salt and scintillator ($C_{10}H_{22}$). In the Baksan ''calorimetric'' experiment [62], the integral muon intensity at the position of the scintillation telescope (8.5 km w.e.) was evaluated from the spectrum of electromagnetic cascades generated by muons in the telescope. To find the muon intensity at the surface, the authors used a conversion procedure similar to that which was used in Refs. [36,37]. As a result of a 10% error in the calibration of the energy evolution in the detector, the systematic error in the determination of the absolute muon intensity can reach 25% in this experiment. One might expect a supplement systematic uncertainty due to the conversion procedure. Comparing with the results of other experiments, the authors moved up their data by 12%. We use the same normalization in Figs. 4(b) and 5(b). The data of Moscow State University (MSU) [64] were extracted from a multidimensional analysis of the measured energy and angular distributions of electron-photon cascades generated by muons in x-ray emulsion chambers. However, the output of this method is also very sensitive to the adopted models for the primary spectrum and charm production. According to Ref. [64], the estimated primary spectrum index is $\gamma_N = 1.64 \pm 0.03$ at nucleon energies 20–400 TeV and the

best-fit X ratio changes from $(2.6 \pm 0.8) \times 10^{-3}$ at $E = 5$ TeV to $(3.3 \pm 1.0) \times 10^{-3}$ at $E = 40$ TeV.

Up to about 5 TeV/c, our prediction for the differential and integral spectra (irrespective of the charm-production model) does not contradict the results of the Artyomovsk detector and the x-ray emulsion chambers of MSU. Below a few TeV the predicted spectrum agrees well with the data from Baksan, Fréjus, and MACRO extracted from the muon DIR, as well as with the Baksan data obtained from the spectrum of electromagnetic cascades [62].

The region from 5 to 15–20 TeV/c is rather oracular: the data of KGF [58], Artyomovsk [60], Baksan [62], and one data point of MSU [64] show a broad dip in the differential and/or integral spectra, whereas the rest of the data indicates some flattening or even a bulge [37].

Above $\sim$20 TeV/c, the data of Baksan [37], MSU [64], and Fréjus [63] clearly indicate a significant flattening of the muon spectrum. Neither the QGSM nor the RQPM can explain this effect; even the maximum VFGS flux is not sufficiently large to this end, although the VFGS flux is not in contradiction with these data. It will be demonstrated in Sec. VII that this flattening is not confirmed by the body of direct underground data, while the late result of KGF [38] seems to be (somewhat) more credible. It is also of interest that, irrespective of the charm-production model, our prediction for the horizontal muon spectrum is in agreement with the corresponding MSU data [64] up to about 40 TeV/c. The KGF spectrum [38] obtained at $X = (9 \pm 2) \times 10^{-4}$ is in qualitative agreement with the RQPM prediction. Apparently the inconsistency of the data from different experiments gives no way of deducing a definite conclusion about the PM fraction in the sea-level muon flux.

VI. MUON PROPAGATION THROUGH MATTER

To calculate the muon depth-intensity relation we apply the semianalytical method proposed in Ref. [124]. The method allows us to avoid any simplifying assumptions about the scale invariance of the cross sections for radiative (direct $e^+ e^-$ pair production, bremsstrahlung) and photonuclear interactions of muons with matter, and to take into account the real non-power-law behavior of the muon boundary spectrum. The solution to the transport equation for the differential muon intensity, $\mathcal{D}_\mu(E, h)$, is constructed by iterations, starting from an initial approximation with the correct high-energy asymptotic behavior. Let us sketch the basic ideas and formulas.

The equation describing the high-energy muon propagation through a homogeneous medium may be written

$$\frac{\partial}{\partial h} \mathcal{D}_\mu(E, h) - \frac{\partial}{\partial E} [\mathcal{B}(E) \mathcal{D}_\mu(E, h)]$$

$$= \sum_{k=p,b,n} \int_0^1 [(1-v)^{-1} \Phi_k(v, E_v) \mathcal{D}_\mu(E_v, h)$$

$$- \Phi_k(v, E) \mathcal{D}_\mu(E, h)] dv, \qquad (6.1)$$

with the boundary condition $\mathcal{D}_\mu(E, 0) = \mathcal{D}_0(E)$. Here $\mathcal{D}_0(E)$ is the ground-level muon spectrum, and $\mathcal{B}$ is the rate of the

muon energy loss which is treated as continuous. In the present calculation, $\mathcal{B}$ includes the ionization energy loss and the part of the loss due to e^+e^- pair production with $v < v_0 = 2 \times 10^{-4}$, where v is the fraction of the energy lost by the muon (see Ref. [125]). However, the method is independent of the specific choice of $\mathcal{B}(E)$. The right-hand side of Eq. (6.1) describes the ''discrete'' muon energy loss resulting from direct e^+e^- pair production with $v > v_0$ ($k=p$), bremsstrahlung ($k=b$), and inelastic nuclear scattering ($k=n$). The corresponding macroscopic cross sections $\Phi_k(v,E)$ are defined by

$$\Phi_k(v,E) = N_0 \frac{d\sigma_k(v,E)}{dv} = N_0 E \frac{d\sigma_k(E,E')}{dE'}\bigg|_{E'=(1-v)E},$$

where N_0 is the number of atoms per 1 g of matter and E (E') is the initial (final) muon energy. It is implied that the differential cross sections are averaged over the atomic number and weight of the target nuclei and $d\sigma_k(v,E)/dv = 0$ outside the ranges $0 \leq v_k^{\min}(E) < v_k^{\max}(E) \leq 1$ allowed by kinematics. Last, $E_v \equiv E/(1-v)$. A summary of the explicit formulas for the cross sections used in our calculation may be found in Ref. [125].

Let us seek a solution of the transport equation (6.1) in the form

$$\mathcal{D}_\mu(E,h) = \mathcal{D}_0(\mathcal{E}_\varrho(E,h)) \exp[-\mathcal{K}(E,h)][1+\delta(E,h)]. \tag{6.2}$$

The functions involved are defined by the following chain of equations:

$$\mathcal{K}(E,h) = \int_E^{\mathcal{E}_\varrho(E,h)} \frac{\xi(E') - \zeta(E')\varrho(E') - \mathcal{B}'(E')}{\mathcal{B}(E') + \varrho(E')E'} dE',$$

$$\varrho(E) = \sum_k \int_0^1 \Phi_k(v,E_v)\eta(v,E)v\,dv,$$

$$\xi(E) = \sum_k \int_0^1 [\Phi_k(v,E) - \eta(v,E)\Phi_k(v,E_v)]dv,$$

$$\zeta(E) = -\frac{E\mathcal{D}_0'(E)}{\mathcal{D}_0(E)}, \qquad \eta(v,E) = \frac{\mathcal{D}_0(E_v)}{(1-v)\mathcal{D}_0(E)}.$$

[As is easy to see, $\zeta = \gamma + 1$ and $\eta(v,E) = (1-v)^\gamma$ in the special case of a power-law boundary spectrum, $\mathcal{D}_0(E) \propto E^{-(\gamma+1)}$.] The function $\mathcal{E}_\varrho(E,h)$ is the only root of the equation

$$\int_E^{\mathcal{E}_\varrho} \frac{dE'}{\mathcal{B}(E') + \varrho(E')E'} = h; \tag{6.3}$$

it can be treated as the effective energy, which a muon must have at the boundary of the medium in order to reach the depth h having energy E with a nonzero probability. Last, the function $\delta(E,h)$ satisfies the equation

$$\left[\frac{\partial}{\partial h} - \mathcal{B}(E)\frac{\partial}{\partial E}\right]\delta(E,h)$$

$$= \sum_k \int_0^1 \Phi_k(v,E_v)\{\Omega(E,E_v,h)[1+\delta(E_v,h)]$$

$$- [1+\omega(E,h)v][1+\delta(E,h)]\}\eta(v,E)dv, \tag{6.4}$$

with

$$\Omega(E,E_v,h) = \frac{\mathcal{D}_0(E)}{\mathcal{D}_0(E_v)} \frac{\mathcal{D}_0(\mathcal{E}_\varrho(E_v,h))}{\mathcal{D}_0(\mathcal{E}_\varrho(E,h))}$$

$$\times \exp[\mathcal{K}(E,h) - \mathcal{K}(E_v,h)],$$

$$\omega(E,h) = \frac{Q(E) - Q(\mathcal{E}_\varrho(E,h))}{\mathcal{B}(E) + \varrho(E)E},$$

$$Q(E) = [\xi(E) - \mathcal{B}'(E)]E + \zeta(E)\mathcal{B}(E).$$

Clearly $\delta(E,0) = 0$. We shall seek the solution to Eq. (6.4) using an iteration procedure. It is based on the following consideration.

Let us suppose that the functions $\Phi_k(v,E)$ and $\zeta(E)$ become energy independent as $E \to \infty$. If so, it is a matter of direct verification to prove that the asymptotic behavior of the function $\delta(E,h)$ is $c_2(h)/E^2$ with $c_2(h)$ an energy-independent function. Hence it follows that $\delta(E_v,h) - (1-v)^2\delta(E,h) \propto (1-v)^2 v E^{-3}$ as $E \to \infty$. Thus, putting $\delta^{(1)}(E,h) = 0$ as a first approximation for the function $\delta(E,h)$, the second one can be found from the equation

$$\left[\frac{\partial}{\partial h} - \mathcal{B}(E)\frac{\partial}{\partial E} - R_2(E,h)\right]\delta^{(2)}(E,h) = \mathfrak{R}_1(E,h),$$

where we introduced

$$R_l(E,h) = \sum_k \int_0^1 \Phi_k(v,E_v)\{\Omega(E,E_v,h)(1-v)^l$$

$$- [1+\omega(E,h)v]\}\eta(v,E)dv, \quad l \geq 0$$

and $\mathfrak{R}_1(E,h) \equiv R_0(E,h)$. Repeating the consideration, one can prove by induction that $\delta(E,h) - \delta^{(l-1)}(E,h) \propto c_l(h)/E^l$ as $E \to \infty$. Let us define

$$\Theta_l(E,h) = \delta^{(l)}(E,h) - \delta^{(l-1)}(E,h), \quad l \geq 2,$$

$$\mathfrak{R}_l(E,h) = \sum_k \int_0^1 \Phi_k(v,E_v)\Omega(E,E_v,h)[\Theta_l(E_v,h)$$

$$- (1-v)^l \Theta_l(E,h)]\eta(v,E)dv, \quad l \geq 2.$$

Then the following recursion chain of equations for the functions $\Theta_l(E,h)$ is derivable from the above reasoning:

$$\left[\frac{\partial}{\partial h} - \mathcal{B}(E)\frac{\partial}{\partial E} - R_l(E,h)\right]\Theta_l(E,h) = \mathfrak{R}_{l-1}(E,h), \quad l \geq 2. \tag{6.5}$$

The solution to Eq. (6.5) is given by

$$\Theta_l(E,h) = \int_0^h \exp\left[\int_{h'}^h R_l[\mathcal{E}_0(E,h-h''),h'']dh'' \right]$$
$$\times \mathfrak{R}_{l-1}[\mathcal{E}_0(E,h-h'),h']dh',$$

where $\mathcal{E}_0(E,h)$ is the root of Eq. (6.3) with $\varrho \equiv 0$ on its left-hand side.

The formal convergence of this procedure can be proved under quite general assumptions on the energy dependence of the functions involved, specifically, if the functions $\mathcal{B}(E)$ and $\Phi_k(v,E)$ increase monotonically and sufficiently slowly, while $\mathcal{D}_0(E)$ decreases with energy so that $\zeta(E)$ is a slightly varying function of energy. It follows from our numerical analysis that in a ''real environment'' the rate of convergence is very high: the first approximation $[\delta(E,h) \equiv 0]$ works with a reasonable exactness up to about 6 km w.e. and three to four iterations are sufficient to obtain a few-percent accuracy for the differential muon spectrum at $h \lesssim 18$ km w.e. and $E \gtrsim 1$ GeV.

The results obtained by the method being discussed agree well with our previous calculations [123]. At $h \lesssim 16$ km w.e. of standard rock, the method was verified by a direct Monte Carlo calculation, using an updated version of the code by Takahashi *et al.* [122]. The accuracy of our calculation for the muon depth-intensity relation,

$$\mathcal{I}_\mu(h) = \int_{E_{th}}^\infty \mathcal{D}_\mu(E,h)dE \quad (E_{th} \sim 1 \text{ GeV}),$$

is estimated to be under (2–3)% at all depths of interest. The systematic errors can only be caused by the uncertainties in the input parameters, namely, the boundary muon spectrum and the muon-matter interaction cross sections. An additional error, arising in the comparison with the data of a particular experiment, is related to the uncertainties in the averaged density and chemical composition of the matter overburden $(\langle \rho \rangle, \langle Z \rangle, \langle A \rangle, \langle Z/A \rangle, \langle Z^2/A \rangle)$ [126]. Strictly speaking, the homogeneous-medium approximation may also introduce a systematic error into the calculation for real inhomogeneous media [127].

VII. CALCULATED MUON DIR vs UNDERGROUND AND UNDERWATER DATA

In Fig. 6, we present a comparison between the calculated vertical intensity (vs depth underground) of conventional muons and the data obtained in early underground experiments performed with relatively small detectors [21–25,28–31] as well as the Crouch's 1987 ''World Survey'' data [49]. To expand the comparison, we represent in Fig. 7 a fragment of the same information relevant to shallow depths.

The data obtained by Wilson [21] and by Clay and Van Gemert [22] in the late 1930s are rather uncertain since the techniques used were unable to estimate the effects of showers, scattering, and δ electrons. We have normalized these data to our curve. All the other data points in Figs. 6 and 7 are absolute. The Crouch World Survey comprises the data of different experiments, in particular, the early KGF data
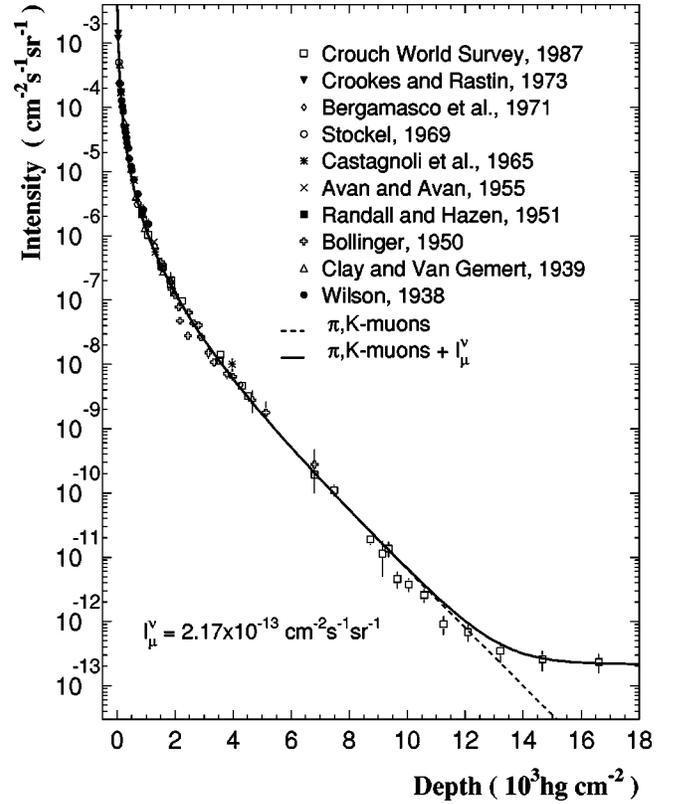
FIG. 6. Muon intensity vs standard rock thickness. The data are from Refs. [21–25,28–31,49]. The dashed curve represents our π,K-muon DIR; the solid curve represents the same plus the neutrino-induced muon background after Crouch [49].

[26,27] and extensive data from East Rand Proprietary Mine (ERPM) near Johannesburg [34] at great depths (all the points at $h \gtrsim 7.5$ km w.e.). All the data were converted by Crouch to standard rock ($Z=11$, $A=22$, $\rho=2.65$ g/cm^3) with some correction for the depths. Crouch's original compilation also includes data from depths well beyond 18 km w.e., where the atmospheric muon contribution is entirely negligible compared to the neutrino-induced muon flux (see below), as well as three data points from an underwater experiment [53] (we dropped these three points, intending to discuss the complete set of underwater data below).

At $h \gtrsim 11$ km w.e., the flux $\mathcal{I}_\mu^\nu$ of muons produced by atmospheric neutrino interactions in the surrounding rock becomes important. The value of $\mathcal{I}_\mu^\nu$ can significantly vary from one experiment to another due to different registration thresholds, the topology of the matter overburden, and so on. So, to account for the neutrino-induced background, we shall use the specific experimental data rather than some theoretical predictions. In Fig. 6 we use the result of Ref. [49]: $\mathcal{I}_\mu^\nu = (2.17 \pm 0.21) \times 10^{-13}$ cm^{-2} s^{-1} sr^{-1}.

According to Crouch, the presented data at $h \gtrsim 1$ km w.e. can be approximated by the following empirical function:

$$\mathcal{I}_\mu(h) = \exp(A_1 + A_2 h) + \exp(A_3 + A_4 h) + \mathcal{I}_\mu^\nu, \quad (7.1)$$

with $A_1 = -11.22 \pm 0.17$, $A_2 = -0.00262 \pm 0.00013$, $A_3 = -14.10 \pm 0.14$, and $A_4 = -0.001213 \pm 0.000021$ (the result
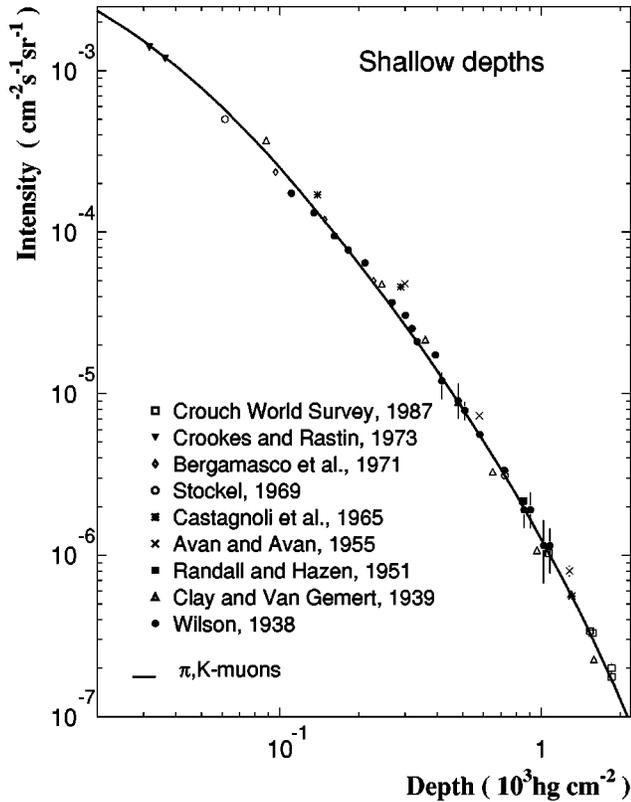
FIG. 7. The same as in Fig. 6 but for shallow depths.

FIG. 8. Muon intensity vs Kolar rock thickness. The KGF data are from Ref. [38]. The curves are for the π,K-muon DIR and for the DIR with the PM contributions calculated according to the RQPM and VFGS model.

of a least squares fit). Here $\mathcal{I}_\mu(h)$ is in $\mathrm{cm}^{-2}\ \mathrm{s}^{-1}\ \mathrm{sr}^{-1}$ and h (the depth in standard rock) is in $\mathrm{hg/cm}^2$ ($1\,\mathrm{hg/cm}^2 = 1$ m w.e.). The fit (7.1) is in good agreement with the result of the Utah group [32].

As Figs. 6,7 suggest, our DIR for conventional muons agrees well with most of the data within a wide depth range from about 30 to 9000 m w.e. (the exceptions are the points from Refs. [25] and [28] at $h \approx 300$ m w.e. and also the points from Ref. [23] lying in the range 2.1–2.5 km w.e.). The maximum disagreement with the best fit (7.1) at $h = 1$–7.5 km w.e. is about 10%. However, at $h = 9.5$–12 km w.e., our intensity noticeably *exceeds* the ERPM data. At $h = 11.5$ km w.e., the disagreement ranges up to about 77% (or about 30%, if one takes the experimental errors into account). Such an error goes far beyond the expected accuracy of our calculations and thus is attributable either to uncertainties in the input parameters (primary spectrum?) or to some systematics in the ERPM data. It is clear that the data give no indication of some PM fraction in the muon flux, and so we do not show the corresponding curves here. As an illustration, let us note that, at $h = 12$ km w.e., the calculated muon intensities with the PM contribution which result from the QGSM, RQPM, and VFGS model are, respectively, 1.7, 2.3, and 3.3 times larger than the Crouch best fit.

Figure 8 shows a comparison with the data obtained from several detectors located at different levels in the deep mine of the Kolar Gold Fields, Mysore State, South India [38] (vertical telescopes at 745, 1500, and 3375 m w.e., a horizontal telescope at 3375 m w.e., and proton decay detectors at 6045 and 7000 m w.e.). In Ref. [38], the neutrino-induced

background has been subtracted from the data using the measured angular distribution of muons. The four curves in Fig. 8 represent our predictions for the muon intensities without and with adding the PM contribution from the QGSM, RQPM, and VFGS model. Our calculations are done for the Kolar rock with $\langle Z \rangle = 12.9$, $\langle A \rangle = 26.9$, $\langle Z/A \rangle = 0.495$, $\langle Z^2/A \rangle = 6.31$, and $\langle \rho \rangle = 3.05$ g/cm^3.

Up to 6–7 km w.e., one can see an excellent agreement between our predictions and the KGF data, irrespective of the PM flux model. Contrary to the data presented in Fig. 6, the KGF muon DIR visibly exceeds the calculated π,K-muon intensity at $h \gtrsim 7$ km w.e., hinting at some PM contribution. Both the RQPM and the VFGS model are in agreement with the KGF data up to about 10 km w.e., but the VFGS model better fits the deeper data. This is not in contradiction with the situation presented in Fig. 5(b) for the sea-level integral spectrum when the ambiguities of the conversion procedure mentioned in Sec. V are taken into account.

In Fig. 9 we show a comparison of the calculation and the data obtained with the Baksan underground scintillation telescope (North Caucasus, Russia). The data obtained at zenith angles $50°$–$70°$ (Ref. [36]) and $70°$–$85°$ (Ref. [37]) were converted by the authors to the vertical direction and to standard rock and the neutrino-induced muon background was subtracted from the data at high depths. A systematic difference between the two sets of data takes place in the depth
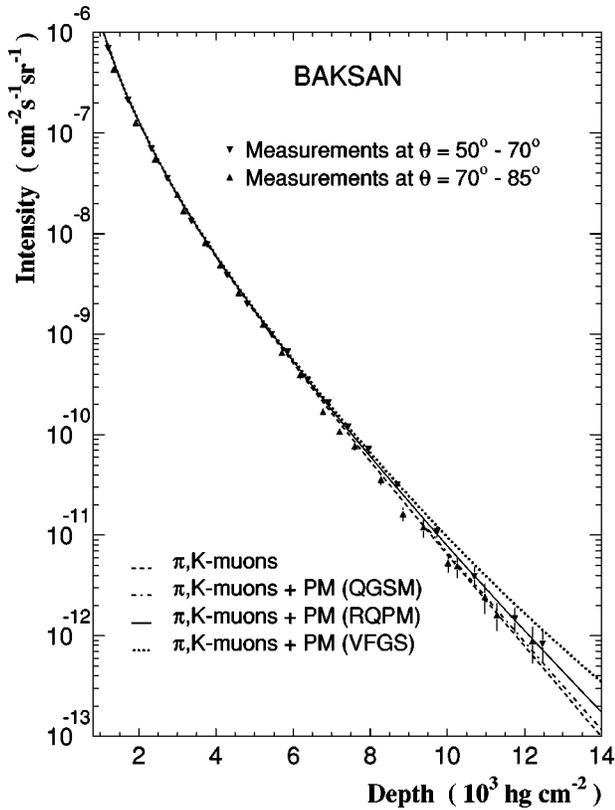
FIG. 9. Muon intensity vs standard rock thickness measured with the Baksan scintillation telescope [36,37]. The notation for the curves is the same as in Fig. 8.

FIG. 10. Single-muon intensity vs standard rock thickness measured in two experiments under Mont Blanc: SCE [35] and NUSEX [41]. The curve is for the predicted π,K-muon DIR.

interval from 6 to 9 km w.e.: in the first set $(50°-70°)$ a bump of intensity is clearly visible, while there is no such bump in the second set of data.

The authors of Ref. [36] argue that the observed bump can be interpreted in terms of prompt muons. In our view this is not the case. The odds are that the bump is caused by errors in the determination of the oblique depths. Beyond the interval 6–9 km w.e., the data of both sets fall on a smooth curve. At the same time, the data at $h \gtrsim 10$ km w.e. may be attributed to the presence of some PM fraction in the measured underground muon intensity. Because of rather large experimental errors, any model of charm production under consideration cannot be excluded by the Baksan data (including the case with a zero PM contribution), but it seems the data are more favorable for the RQPM. A collation of Figs. 9 and 5(b) suggests that the sea-level integral spectrum reconstructed in Ref. [37] from the Baksan muon DIR was distinctly overestimated.

Figure 10 shows the comparison of the predicted DIR for the conventional muons with the *single-muon* intensity measured with the detectors SCE and NUSEX [35,41] located in the Mont Blanc Laboratory. Our calculation represents the muon intensity averaged upon the muon multiplicities and therefore we can make nothing more than qualitative conclusions from the comparison.

In the overlapping region $(h \lesssim 7$ km w.e.) the data of both detectors superimpose and (with allowance for the multimuon events) agree with our result. However, as is

clear from the figure, the NUSEX DIR has a much greater abrupt grade compared with the predicted one for the π,K-muon DIR and, at 9–11 km w.e., the predicted intensity (without any PM contribution) is 2–3 times higher than the NUSEX data. So large a discrepancy has no relation to the multimuon events, whose intensity decreases with depth quicker than the single-muon one and is negligible at $h > 6-7$ km w.e. within a few percent accuracy.

It is our opinion that the NUSEX result at large depths is incorrect. Notice that the muon DIR measured in the NUSEX experiment has been converted to standard rock. Although the averaged values of ρ, Z, A, Z/A, and Z^2/A in the Mont Blanc rock are rather close to the "standard" ones, this conversion might be a serious source of a systematic error because of very complicated and heterogeneous (layered) chemical composition of the rock (see Ref. [35]).

We note here that our calculations are in good agreement with the result of the French-American muon experiment [33] also carried out in the Mt. Blanc tunnel with a GM telescope. The depth range explored in that experiment was 0.5–5 km w.e. and therefore overlaps in part the SCE-NUSEX depth range. This suggests that the SCE and NUSEX experiments may have an added source of systematics related to their experimental procedures.

Figure 11 represents the comparison of our prediction with the data from SOUDAN 1 and SOUDAN 2 underground experiments [42,43] (the data points are taken from the compilation presented in Ref. [44]). The SOUDAN data
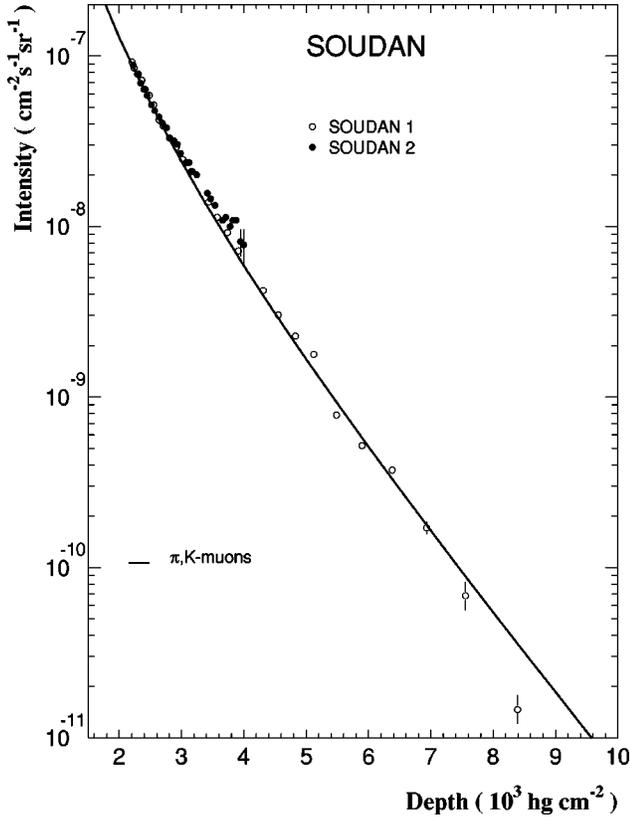
FIG. 11. Muon intensity vs standard rock thickness measured in the SOUDAN 1 and SOUDAN 2 experiments [42,43]. The curve is for the predicted π,K-muon DIR.

FIG. 12. Muon intensity vs standard rock thickness measured in the Fréjus experiment [39]. The dashed curve represents our π,K-muon DIR; the solid curve represents the same plus the neutrino-induced muon background, $\mathcal{I}_{\mu}^{\nu}$, according to Ref. [40]. The other curves are for the muon DIR with the PM contributions calculated according to the RQPM and VFGS model plus $\mathcal{I}_{\mu}^{\nu}$.

were normalized to the DIR for standard rock using the Crouch World Survey, as described in Ref. [43].

Despite some spread of experimental points and a bump at 3–4 km w.e., one can see a reasonable agreement between the calculated π,K-muon DIR and the data up to about 7 km w.e., but the last point ($\sim$8.4 km w.e.) is almost 2.5 times below the predicted curve, as in the case of the NUSEX data.

In Fig. 12, we compare our calculations with the data of the Fréjus detector [39] (the underground laboratory was located in a tunnel of the same name under the Alps). The Alpine rock thickness has been converted into hg/cm^2 of standard rock. We do not include in our assemblage the new and very detailed data from the Fréjus detector recently reanalyzed in Ref. [40] (see also Ref. [63]). The point is that the original data sample has been subdivided into throughgoing, multiple, and stopping muons. These subsamples are very dependent of the features peculiar to the experiment and thus cannot be directly compared with our calculations.

According to Ref. [40], the neutrino-induced muon background becomes dominant at $h \gtrsim 13$ km w.e. and the measured mean background flux is $\mathcal{I}_{\mu}^{\nu}=(3.67\pm0.66)\times10^{-13}$ cm^{-2} s^{-1} sr^{-1}. One can see that the intensity calculated without the PM contribution and corrected for this background fits the Fréjus data almost everywhere, although in the vicinity of $h=10$ km w.e. some hint of an excess over the data (similar to the more evident excess in ERPM and NUSEX) does take place. The PM contributions calculated with the RQPM and the VFGS model do not fall into the Fréjus

data. However, in view of the experimental uncertainties there is no telling that the RQPM prediction is in serious conflict with the Fréjus result. Clearly the same is all the more true for the VFGS model.

The recent data from the two largest underground detectors MACRO [44] and LVD [128] (located in the Gran Sasso Laboratory) are presented in Figs. 13 and 14, respectively. The data of MACRO are converted to standard rock. The error bars include the statistical uncertainty, the systematic uncertainty for the topographical map, and the additional estimated systematic scale uncertainty of $\pm8\%$. Taken alone, the statistical errors in the MACRO experiment are very small. The main contribution to the absolute scale uncertainty comes from the assumption of a homogeneous mountain instead of a layered structure. The data of LVD are presented both for the Gran Sasso rock and standard rock. Errors include both statistical and systematic uncertainties. Notice that at $h \lesssim 5$ km w.e., the statistical errors are less than the size of the circles in the figure.

The depths currently accessible for observation with the detector MACRO are insufficient to study prompt muons. Thus, in Fig. 13 we present the calculated π,K-muon DIR alone. In contrast, the LVD data (Fig. 14) overlap the total depth range where the PM contribution might be essential. We use for our calculated curves the following value of the
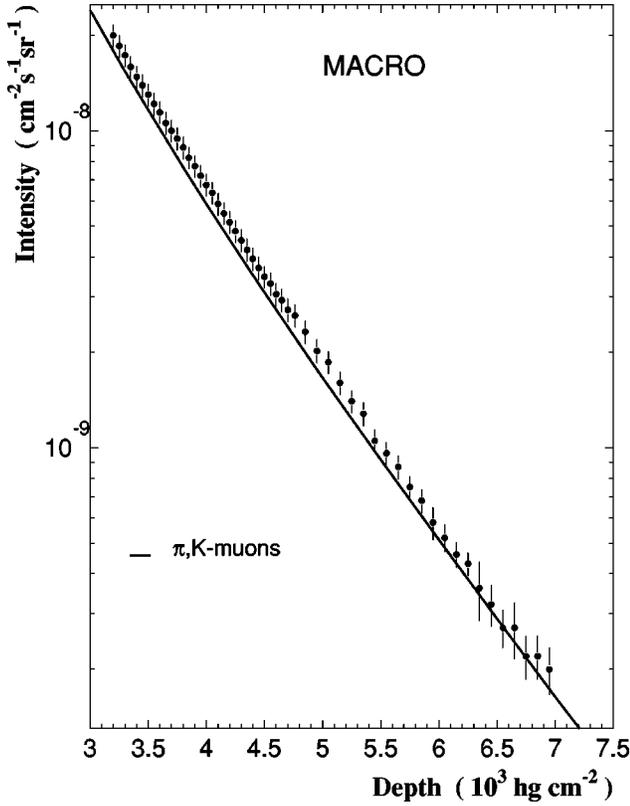
FIG. 13. Muon intensity vs standard rock thickness measured in the experiment MACRO [44]. The curve is for the calculated π,K-muon DIR.

FIG. 14. Muon intensity vs standard rock and Gran Sasso rock thickness [128]. The notation of the curves is the same as in Fig. 12 but with the neutrino-induced muon contribution $\mathcal{I}_\mu^\nu$ deduced in Ref. [45].

neutrino-induced muon background: $\mathcal{I}_\mu^\nu = (2.98 \pm 1.15) \times 10^{-13}$ cm^{-2} s^{-1} sr^{-1} [45].

As Fig. 13 suggests, in the range from 3200 to about 6000 hg/cm^2 the MACRO data are systematically in excess of our predicted muon intensity by about (8–10)%, which is beyond the total systematic error estimated in Ref. [44]. This fact seems to be in dramatic contradiction with the sea-level muon spectrum reconstructed from the MACRO underground data under discussion (see Fig. 4). Indeed, our sea-level spectrum of the π,K muons is in good agreement with the MACRO fit (5.1) of the sea-level spectrum from 600–700 GeV up to 6–7 TeV and it *stands out above* the MACRO fit at higher energies. However, as noted in Sec. V, the overall systematic error of the fit (5.1) is large enough to explain this contradiction, at least formally.

At all depths, the LVD data are in excellent agreement with our calculations for the conventional muon DIR. Therefore, the data favor the models of charm production which predict a very low PM contribution (QGSM, PQCD, DPM). The consistency of the data with our calculations for standard and Gran Sasso rocks provides an important confirmation for the correctness of the new conversion procedure to standard rock used in the LVD analysis [46].

Some problems of the underground muon experiments can be overcome by measurements underwater (and "underice") owing to the unlimited (in principle) detection volume, uniformity and well-known composition of the matter overburden.

We present the total (to our knowledge) assemblage of underwater data in Fig. 15. The measurements with compact closed installations were performed in Suruga-bay, West Pacific (Higashi *et al.* [50]), in Lake Geneva (Rogers and Tristam [52]), and in the Atlantic Ocean, Black, Mediterranean, and Caribbean Seas during several expeditions of research ships (Davitaev *et al.* [51], Fyodorov *et al.* [53]). The measurements with open detectors (strings with phototubes), the prototypes of future large-scale neutrino telescopes, were performed in the Pacific Ocean off the West coast of the island of Hawaii in 1987 (the DUMAND Short Prototype String, Babson *et al.* [54]), in the Mediterranean Sea a short way off Pylos, during three expeditions in 1989, 1991, and 1992 (the NESTOR prototypes, Anassontzis *et al.* [55]), and in Lake Baikal during two expeditions in 1992 and 1993 (the stationary prototypes of the underwater neutrino telescope NT-200, Belolaptikov *et al.* [56,57]).

Our calculation for the π,K-muon DIR was done for sea water with $\langle Z \rangle = 7.468$, $\langle A \rangle = 14.87$, $\langle Z/A \rangle = 0.5525$, $\langle Z^2/A \rangle = 3.770$, and $\langle \rho \rangle = 1.027$ g/cm^3. At $h \lesssim 7$ km, the difference with the DIR for pure H$_2$O is less than 1% and can be neglected as compared to the theoretical and experimental uncertainties.

At shallow depths (to 175 m) there are two measurements with very good statistics (Higashi *et al.* [50,52], Rogers and Tristam [52]), but the results of Higashi *et al.* are lower by (15–30)% than the result of Rogers and Tristam. According to Ref. [52], one reason for the discrepancy is believed to be
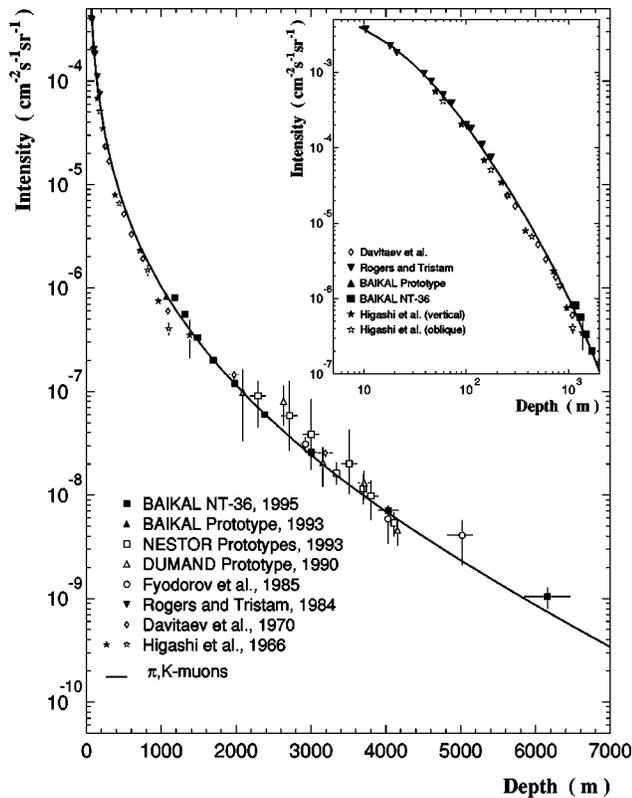
FIG. 15. Muon intensity vs depth in water. The data of underwater experiments are from Refs. [50–57]. The curve is for the calculated π,K-muon DIR.

as follows. Higashi *et al.* normalized their data to an intensity derived from earlier underground measurements and measurements of the sea-level muon spectrum. The intensity chosen for the normalization is not quoted in Ref. [50], but was almost certainly too low. Our prediction is in excellent agreement with the absolute intensity obtained by Rogers and Tristam. This provides good support of our nuclear-cascade model at low energies. However, the absolute measurements of Davitaev *et al.* [51] are systematically lower than our prediction at $h \lesssim 1$ km.

As for greater depths, 1–4 km, it can be concluded that our prediction is in tolerable agreement with the data from the DUMAND and NESTOR prototypes as well as with the data of Fyodorov *et al.*; the discrepancy with a few specific data points is within $(1-1.5)\sigma$ and is compatible with the overall data scattering. The data of the Baikal Collaboration [56,57] (the most statistically valid) are in very good agreement with our curve.

As is evident from the foregoing, the present-day state of large-scale underwater projects does not permit one to compete with the underground detectors as yet. In particular, the (slant) depths explored by the present-day underwater experiments are too small to get useful information on the PM flux.

VIII. CONCLUSIONS

In this work we have attempted to study the vertical flux of high-energy cosmic-ray muons ''from top to bottom,''

that is, from the primary spectrum of cosmic rays to underground and underwater muon intensity. Based upon the comparison of our calculations with the present-day ground-level, underground, and underwater measurements, we have reached the following conclusions.

Below 1 TeV/c, the spread of the data on the vertical sea-level muon spectra (differential and integral) measured in different experiments runs up to about 50% and it is as much as (25–30)% even among the data of absolute measurements. Our calculations in this momentum range most closely fit the absolute 1984 data from the Nottingham magnetic spectrograph [14]. Below 5–6 TeV/c, they agree with the indirect data deduced in most of the underground experiments (Artyomovsk [60], Baksan [37,62], MACRO [44], Fréjus [63], MSU [64]) *without reference to a charm-production model.* At higher energies, the (indirect) sea-level data become contradictory to an extent that they give no way to make any definite conclusion about the validity of our nuclear-cascade model and to choose among the charm-production models under consideration. In particular, above ~ 20 TeV/c, the data on the muon differential spectrum suggest a very high PM flux (as predicted by the VFGS model or even higher). At the same time, the data on the integral spectrum from different groups require different rates for charm production and cannot be described by a single nuclear-cascade model.

At depths from about 30 m w.e. up to 6–7 km w.e., essentially all underground data on the muon DIR correlate with each other and with the predicted intensity for conventional (π,K) muons, to within 10%. Hence it follows that our nuclear-cascade model is valid with the same precision from about 8 GeV up to 4–5 TeV of muon energy at sea level, i.e., up to about 100 TeV/nucleon in the primary spectrum. This precision is distinctly better than one might expect with the uncertainties in the input parameters (including the primary spectrum model and the muon-matter interaction cross sections). It is important that the underground data at $h < 6$–7 km w.e. do more than correlate well, but they also have a very good statistical accuracy. Therefore, they may be of utility, among other things, for a normalization of the atmospheric neutrino flux just in the range of neutrino energies most essential for ν-induced muons.

The present-day world underwater results, though moderately detailed, provide a very important check upon the accuracy of the underground experiments, since they are free of the uncertainties in the density and composition of the matter overburden. The data obtained with the prototypes of future large underwater neutrino telescopes, and especially with the Baikal NT-36, are in good agreement with the underground data and with our calculations.

The situation with the underground data at $h \gtrsim 7$ km w.e. is unsatisfactory in the same sense that it is with the ground-level data at high energies. The data from KGF [38] and also from Baksan [36] (measurements at $\vartheta = 50° - 70°$) demonstrate clear *excess* over the predicted π,K-muon curve, providing fair indication of PM production. In contrast, the data points from ERPM [34,49] and especially from NUSEX [41] are *under* the π,K-muon curve. The data of all the other underground experiments are between these extremes. As a

result, no undisputed conclusion about PM production can be extracted from the world underground data. Considering that the statistical significances of the underground results at great depths are comparable and quite tolerable, this situation is attributable to the fact that certain of the experiments discussed have unrecorded systematic uncertainties.

[1] A. De Rújula, E. Fernández, and J. J. Gómez-Cadenas, Nucl. Phys. **B405**, 80 (1993).

[2] T. K. Gaisser, F. Halzen, and T. Stanev, Phys. Rep. **258**, 173 (1995).

[3] E. V. Bugaev, V. A. Naumov, S. I. Sinegovsky, and E. S. Zaslavskaya, Nuovo Cimento C **12**, 41 (1989).

[4] E. Zas, F. Halzen, and R. A. Vázquez, Astropart. Phys. **1**, 297 (1993); M. C. Gonzalez-Garcia, F. Halzen, R. A. Vázquez, and E. Zas, Phys. Rev. D **49**, 2310 (1994).

[5] M. Thunman, G. Ingelman, and P. Gondolo, in *Proceedings of the Workshop on Trends in Astroparticle Physics*, Stockholm, Sweden, 1994, edited by L. Bergström *et al.* [Nucl. Phys. B (Proc. Suppl.) **43**, 274 (1995)]; P. Gondolo, G. Ingelman, and M. Thunman, Astropart. Phys. **5**, 309 (1996)].

[6] W. Frati, T. K. Gaisser, A. K. Mann, and T. Stanev, Phys. Rev. D **48**, 1140 (1993); D. H. Perkins, Nucl. Phys. **B399**, 3 (1993); T. K. Gaisser, M. Honda, K. Kasahara, H. Lee, S. Midorikawa, V. A. Naumov, and T. Stanev, Phys. Rev. D **54**, 5578 (1996).

[7] A. M. Aurela and A. W. Wolfendale, Proc. Phys. Soc. London **81**, 593 (1963).

[8] S. R. Baber, W. F. Nash, and B. C. Rastin, Nucl. Phys. **B4**, 539 (1968).

[9] B. J. Bateman *et al.*, Phys. Lett. **36B**, 144 (1971).

[10] O. C. Allkofer, K. Carstensen, and W. D. Dau, Phys. Lett. **36B**, 425 (1971).

[11] B. C. Nandi and M. S. Sinha, J. Phys. A **5**, 1384 (1972).

[12] C. A. Ayre *et al.*, J. Phys. G **5**, 584 (1975).

[13] M. G. Thompson *et al.*, in *Proceedings of the 15th International Cosmic Ray Conference*, Plovdiv, 1977, edited by C. Ya. Christov *et al.* (Institute for Nuclear Research, Bulgarian Academy of Sciences, Sofia, 1977), Vol. 6, p. 21.

[14] B. C. Rastin, J. Phys. G **10**, 1609 (1984).

[15] M. P. De Pascale *et al.*, J. Geophys. Res. **98**, 3501 (1993).

[16] M. Bruscoli and M. Pieri, INFN, Sezione di Firenze, Report No. DFF 182/2/93, 1993 (unpublished). See also P. Le Coultre, in *Proceedings of the 3rd NESTOR International Workshop*, Fortress of Niokastro, Pylos, Greece, 1993, edited by L. K. Resvanis (Physics Laboratory, University of Athens, Athens, 1994), p. 253.

[17] EAS-TOP Collaboration, M. Aglietta *et al.*, in Proceedings of the 24th International Cosmic Ray Conference, Roma, Italy, 1995 (unpublished), Vol. 1, p. 638.

[18] S. Matsuno *et al.*, Phys. Rev. D **29**, 1 (1984).

[19] O. C. Allkofer *et al.*, Nucl. Phys. **B259**, 1 (1985).

[20] O. C. Allkofer and P. K. F. Grieder, *Cosmic Rays on Earth* (Fachsinformationszentrum, Karlsruhe, 1984).

[21] V. C. Wilson, Phys. Rev. **53**, 337 (1938).

[22] J. Clay and A. Van Gemert, Physica **6**, 497 (1939).

[23] L. M. Bollinger, Ph.D. thesis, Cornell University, 1951; Phys. Rev. **79**, A207 (1950) (abstract, no results); results are presented in P. H. Barrett *et al.*, Rev. Mod. Phys. **24**, 133 (1952).

[24] C. A. Randall and W. E. Hazen, Phys. Rev. **81**, 144 (1951).

[25] L. Avan and M. Avan, Compt. Rend. **241**, 1122 (1955).

[26] S. Miyake, V. S. Narasimham, and P. V. Ramana Murthy, Nuovo Cimento **32**, 1505 (1964).

[27] S. Miyake, V. S. Narasimham, and P. V. Ramana Murthy, Nuovo Cimento **35**, 969 (1965); M. R. Krishnaswamy *et al.*, in *Proceedings of the 11th International Cosmic Ray Conference*, Budapest, Hungary, 1969, edited by T. Gémsey *et al.* [Acta Phys. Acad. Sci. Hung. **29**, Suppl. 4, 221 (1970)]; M. R. Krishnaswamy *et al.*, Proc. R. Soc. London **A323**, 511 (1971).

[28] C. Castagnoli, A. De Marco, A. Longhetto, and P. Penego, Nuovo Cimento **35**, 969 (1965).

[29] C. T. Stockel, J. Phys. A **2**, 639 (1969).

[30] L. Bergamasco, B. D'Ettore Piazzoli, and P. Picchi, Nuovo Cimento B **4**, 59 (1971).

[31] J. N. Crookes and B. C. Rastin, Nucl. Phys. **B58**, 93 (1973). Together with the original results, this paper includes a particular compilation of the data from early underground experiments at shallow depths.

[32] G. L. Cassiday, J. W. Keuffel, and J. A. Thompson, Phys. Rev. D **7**, 2022 (1973); G. W. Carlson, Ph.D. thesis, University of Utah, 1972.

[33] W. R. Sheldon *et al.*, Phys. Rev. D **17**, 114 (1978).

[34] B. S. Meyer *et al.*, Phys. Rev. D **1**, 2229 (1970); M. F. Crouch *et al.*, *ibid.* **18**, 2239 (1978).

[35] C. Castagnoli and O. Saavedra, Nuovo Cimento C **9**, 111 (1986).

[36] Yu. M. Andreyev, V. I. Gurentsov, and I. M. Kogai, in *Proceedings of the 20th International Cosmic Ray Conference*, Moscow, USSR, 1987, edited by V. A. Kozyarivsky *et al.*

(Nauka, Moscow, 1987), Vol. 6, p. 200.

[37] Yu. M. Andreyev, A. E. Chudakov, V. I. Gurentsov, and I. M. Kogai, in *Proceedings of the 21st International Cosmic Ray Conference*, Adelaide, Australia, 1990, edited by R. J. Protheroe (Department of Physics and Mathematical Physics, University of Adelaide, Northfield, South Australia, 1990), Vol. 9, p. 301; Yu. M. Andreyev (private communication).

[38] KGF Collaboration, N. Ito *et al.*, in *Proceedings of the International Symposium on Underground Physics Experiment*, Tokyo, Japan, 1990, edited by K. Nakamura (ICRR, Tokyo, 1990), p. 101.

[39] Fréjus Collaboration, Ch. Berger *et al.*, Phys. Rev. D **40**, 2163 (1989); Z. Phys. C **48**, 221 (1990).

[40] Fréjus Collaboration, W. Rhode *et al.*, Astropart. Phys. **4**, 217 (1996).

[41] NUSEX Collaboration, M. Aglietta *et al.*, in *Proceedings of the Topical Seminar ''Astrophysics and Particle Physics,''* San Miniato, Italy, 1989, edited by G. Castellini *et al.* [Nucl. Phys. B (Proc. Suppl.) **14B**, 193 (1990)].

[42] SOUDAN Collaboration, Internal Report No. PDK-435, 1990 (unpublished).

[43] S. M. Kasahara, Ph.D. thesis, University of Minnesota, 1995.

[44] MACRO Collaboration, M. Ambrosio *et al.*, Phys. Rev. D **52**, 3793 (1995).

[45] LVD Collaboration, M. Aglietta *et al.*, Astropart. Phys. **3**, 311 (1995).

[46] LVD Collaboration, G. P. Sartorelli, in *Proceedings of the 25th International Cosmic Ray Conference*, Durban, South Africa, 1997, edited by M. S. Potgieter, B. C. Raubenheimer, and D. J. van der Walt (Wesprint, Potchefstroom, 1997), Vol. 6, p. 341.

[47] M. G. K. Menon and P. V. Ramana Murthy, in *Progress in Elementary Particle and Cosmic Ray Physics*, edited by J. G. Wilson and S. A. Wouthuysen (North-Holland, Amsterdam, 1967), Vol. 9, Chap. 3, p. 163; G. L. Cassiday, J. W. Keuffel, and J. A. Thompson, Phys. Rev. D **7**, 2022 (1973); A. I. Barbouti and B. C. Rastin, J. Phys. G **9**, 1577 (1983).

[48] E. V. Bugaev, Yu. D. Kotov, and I. L. Rozental, *Cosmic Muons and Neutrinos* (Atomizdat, Moscow, 1970).

[49] M. F. Crouch, in *Proceedings of the 20th International Cosmic Ray Conference* [36], Vol. 6, p. 165.

[50] S. Higashi *et al.*, Nuovo Cimento A **43**, 334 (1966).

[51] L. N. Davitaev, V. M. Fyodorov, Yu. A. Trubkin, and Yu. N. Vavilov, in *Proceedings of the 11th International Cosmic Ray Conference* [27], p. 53; Yu. N. Vavilov, L. N. Davitaev, Yu. A. Trubkin, and V. M. Fyodorov, Izv. Akad. Nauk SSSR, Ser. Fiz. **2**, 1977 (1970) [Bull. Acad. Sci. USSR, Phys. Ser. **34**, 1759 (1970)]; see also Yu. N. Vavilov, Yu. A. Trubkin, and V. M. Fyodorov, Yad. Fiz. **18**, 844 (1974) [Sov. J. Nucl. Phys. **18**, 434 (1974)].

[52] I. W. Rogers and M. Tristam, J. Phys. G **10**, 983 (1984).

[53] V. M. Fyodorov, V. P. Pustovetov, Yu. A. Trubkin, and A. V. Kirilenkov, in *Proceedings of the 19th International Cosmic Ray Conference*, La Jolla, CA, 1985, edited by F. C. Jones *et al.* (Scientific and Technical Information Branch, NASA, U.S. GPO, Washington, D.C., 1985), Vol. 8, p. 39; V. M. Fyodorov, Nucl. Instrum. Methods Phys. Res. A **248**, 221 (1986).

[54] DUMAND Collaboration, J. Babson *et al.*, Phys. Rev. D **42**, 3613 (1990).

[55] NESTOR Collaboration, E. G. Anassontzis *et al.*, in *Proceedings of the 23rd International Cosmic Ray Conference*, Calgary, Canada, 1993, edited by D. A. Leahy (Department of Physics and Astronomy, University of Calgary, Calgary, 1993), Vol. 4, p. 554.

[56] Baikal Collaboration, I. A. Belolaptikov *et al.*, in *Proceedings of the 23rd International Cosmic Ray Conference* [55], Vol. 4, p. 573; in *Proceedings of the 2nd NESTOR International Workshop*, Fortress of Niokastro, Pylos, Greece, 1992, edited by L. K. Resvanis (Physics Laboratory, University of Athens, Athens, 1993), p. 238; Astropart. Phys. **7**, 263 (1997).

[57] Baikal Collaboration, I. A. Belolaptikov *et al.*, in Proceedings of the 24th International Cosmic Ray Conference [17], Vol. 1, p. 536; Astropart. Phys. **7**, 263 (1997).

[58] S. Miyake, V. S. Narasimham, and P. V. Ramana Murthy, Nuovo Cimento **32**, 1523 (1964).

[59] M. R. Krishnaswamy *et al.*, Nuovo Cimento C **9**, 167 (1986).

[60] F. F. Khalchukov *et al.*, in *Proceedings of the 19th International Cosmic Ray Conference* [53], Vol. 8, p. 12.

[61] KGF Collaboration, H. Adarkar *et al.*, in *Proceedings of the 21st International Cosmic Ray Conference* [37], Vol. 9, p. 310.

[62] V. N. Bakatanov *et al.*, Yad. Fiz. **55**, 2107 (1992) [Sov. J. Nucl. Phys. **55**, 1169 (1992)].

[63] W. Rhode, in *TAUP'93*, Proceedings of the 3rd International Workshop on Theoretical and Phenomenological Aspects of Underground Physics, Gran Sasso, Italy, 1993, edited by C. Arpesella, E. Bellotti, and A. Bottino [Nucl. Phys. B (Proc. Suppl.) **35**, 250 (1994)]; see also W. Rhode, Ph.D. thesis, Wuppertal University, 1993.

[64] G. T. Zatsepin *et al.*, Izv. Ross. Akad. Nauk, Ser. Fiz. **58**, 119 (1994) [Bull. Russ. Acad. Sci., Phys. Ser. **58**, 2050 (1994)]; E. A. Osipova (private communication).

[65] For some preliminary results, see V. A. Naumov, T. S. Sinegovskaya, and S. I. Sinegovsky, Università degli Studi di Firenze, Report No. DFF 253/06/1996, 1996 (unpublished); Report No. hep-ph/9802410 [Nuovo Cimento A (to be published)]; A. Misaki, V. A. Naumov, T. S. Sinegovskaya, and S. I. Sinegovsky, in *Proceedings of the 25th International Cosmic Ray Conference* [46], Vol. 7, p. 129.

[66] S. N. Nikol'sky, I. I. Stamenov, and S. Z. Ushev, Zh. Éksp. Teor. Fiz. **87**, 18 (1984) [Sov. Phys. JETP **60**, 10 (1984)]. See also S. N. Nikol'sky, in *Problems of Cosmic Ray Physics*, edited by A. E. Chudakov *et al.* (Nauka, Moscow, 1987), p. 169.

[67] I. P. Ivanenko *et al.*, in *Proceedings of the 21st International Cosmic Ray Conference* [37], Vol. 2, p. 17.

[68] JACEE Collaboration, K. Asakimori *et al.*, in *Proceedings of the 22nd International Cosmic Ray Conference*, Dublin, Ireland, 1991, edited by M. Cawley *et al.* (The Dublin Institute for Advanced Studies, Dublin, 1991), Vol. 2, pp. 57 and 97.

[69] M. Teshima, in *Proceedings of the 23rd International Cosmic Ray Conference* [55], Invited, Rapporteur, and Highlight Papers, p. 257.

[70] M. Ichimura *et al.*, Phys. Rev. D **48**, 1949 (1993); in *Proceedings of the 23rd International Cosmic Ray Conference* [55], Vol. 2, p. 5.

[71] P. Sokolsky, P. Sommers, and B. R. Dawson, Phys. Rep. **217**,

225 (1992); T. V. Danilova, A. D. Erlykin, and J. Procureur, Yad. Fiz. **55**, 2968 (1992) [Sov. J. Nucl. Phys. **55**, 1659 (1992)]; X. Chi, M. N. Vahia, J. Wdowczyk, and A. W. Wolfendale, J. Phys. G **18**, 553 (1992); V. I. Zatsepin, T. V. Lazareva, G. P. Sazhina, and N. V. Sokol'skaya, Yad. Fiz. **57**, 684 (1994) [Phys. At. Nucl. **57**, 645 (1994)]; L. I. Vil'danova, N. M. Nesterova, and A. P. Chubenko, *ibid.* **57**, 2231 (1994); [**57**, 2245 (1994)].

[72] A. N. Vall, V. A. Naumov, and S. I. Sinegovsky, Yad. Fiz. **44**, 1240 (1986) [Sov. J. Nucl. Phys. **44**, 806 (1986)].

[73] Y. Minorikawa, Lett. Nuovo Cimento **22**, 247 (1974); Y. Minorikawa and K. Mitsui, *ibid.* **41**, 333 (1984).

[74] V. V. Anisovich, V. M. Braun, and Yu. M. Shabel'sky, Yad. Fiz. **39**, 932 (1984) [Sov. J. Nucl. Phys. **39**, 590 (1984)].

[75] V. A. Naumov, in *Investigations on Geomagnetism, Aeronomy, and Solar Physics* (Nauka, Moscow, 1984), Vol. 73, p. 198; E. V. Bugaev and V. A. Naumov, Institute for Nuclear Research, Academy of Sciences of the USSR, Report Nos. Π-0385 and Π-0401, 1985 (unpublished).

[76] E. V. Bugaev and V. A. Naumov, Yad. Fiz. **45**, 1380 (1987) [Sov. J. Nucl. Phys. **45**, 857 (1987)]. See also E. V. Bugaev and V. A. Naumov, Institute for Nuclear Research, Academy of Sciences of the USSR, Report No. Π-0537, 1987 (unpublished); V. A. Naumov, in *Proceedings of the International Workshop on ν_μ/ν_e Problem in Atmospheric Neutrinos*, Gran Sasso, Italy, 1993, edited by V. S. Berezinsky and G. Fiorentini (LNGS, L'Aquila, Italy, 1993), p. 25.

[77] It is pertinent to note that the $K_{\mu 3}$ decays contribute significantly to the atmospheric neutrino flux, and what is more, the inclusion of $K_{\ell 3}$ form factors noticeably affects the neutrino flavor ratio at high energies (see Ref. [65]).

[78] L. V. Volkova, G. T. Zatsepin, and L. A. Kuz'michev, Yad. Fiz. **29**, 1252 (1979) [Sov. J. Nucl. Phys. **29**, 645 (1979)].

[79] A. Dar, Phys. Rev. Lett. **51**, 227 (1983); in *Proceedings of the 4th International Workshop on Grand Unification*, Philadelphia, 1983, edited by P. Langacker and P. J. Steinhardt (Birkhäuser, Boston, 1983), p. 101.

[80] A. V. Butkevich, L. G. Dedenko, and I. M. Zheleznykh, Yad. Fiz. **50**, 142 (1989) [Sov. J. Nucl. Phys. **50**, 90 (1989)].

[81] P. Lipari, Astropart. Phys. **1**, 195 (1993).

[82] V. Agrawal, T. K. Gaisser, P. Lipari, and T. Stanev, Phys. Rev. D **53**, 1314 (1996).

[83] H. Inazawa and K. Kobayakawa, Prog. Theor. Phys. **69**, 1195 (1983).

[84] J. W. Elbert, T. K. Gaisser, and T. Stanev, Phys. Rev. D **27**, 1448 (1983).

[85] L. V. Volkova and G. T. Zatsepin, Yad. Fiz. **37**, 353 (1983) [Sov. J. Nucl. Phys. **37**, 212 (1983)]; Izv. Akad. Nauk SSSR, Ser. Fiz. **49**, 1386 (1985) [Bull. Acad. Sci. USSR, Phys. Ser. **49**, 143 (1985)].

[86] C. Castagnoli *et al.*, Nuovo Cimento C **8**, 78 (1984).

[87] Y. Minorikawa and K. Mitsui, Lett. Nuovo Cimento **44**, 651 (1985); K. Mitsui, Y. Minorikawa, and H. Komori, Nuovo Cimento C **9**, 995 (1986).

[88] H. Inazawa, K. Kobayakawa, and T. Kitamura, J. Phys. G **12**, 59 (1986); Nuovo Cimento C **9**, 382 (1986).

[89] O. C. Allkofer and D. P. Bhattacharyya, Astrophys. Space Sci. **134**, 115 (1987).

[90] L. V. Volkova, W. Fulgione, P. Galeotti, and O. Saavedra, Nuovo Cimento C **10**, 465 (1987).

[91] E. V. Bugaev, V. A. Naumov, S. I. Sinegovsky, and E. S. Zaslavskaya, in *Proceedings of the 20th International Cosmic Ray Conference* [36], Vol. 6, p. 305; Institute for Nuclear Research, Academy of Sciences of the USSR, Report No. Π-0568, 1987 (unpublished).

[92] E. V. Bugaev, V. A. Naumov, S. I. Sinegovsky, and E. S. Zaslavskaya, Izv. Akad. Nauk SSSR, Ser. Fiz. **53**, 342 (1989) [Bull. Acad. Sci. USSR, Phys. Ser. **53**, 135 (1989)].

[93] M. Treichel, Z. Phys. C **54**, 469 (1992).

[94] G. Battistoni, C. Bloise, C. Forti, M. Greco, J. Ranft, and A. Tanzini, Astropart. Phys. **4**, 351 (1996).

[95] P. Pal, D. P. Bhattacharyya, and S. Bhattacharyya, Nuovo Cimento C **17**, 255 (1994).

[96] A. B. Kaidalov and O. I. Piskunova, Yad. Fiz. **41**, 1278 (1985) [Sov. J. Nucl. Phys. **41**, 816 (1985)]; **43**, 1545 (1986) [**43**, 994 (1986)]; Z. Phys. C **30**, 145 (1986); O. I. Piskunova, Yad. Fiz. **56**, 176 (1993) [Sov. J. Nucl. Phys. **56**, 1094 (1993)].

[97] See, e.g. G. Anzivino *et al.*, Nuovo Cimento A **107**, 955 (1994) and references therein.

[98] H. Nowak, Fortschr. Phys. **39**, 347 (1991); J. A. Appel, Annu. Rev. Nucl. Part. Sci. **42**, 367 (1992); G. Anzivino *et al.*, Nuovo Cimento A **107**, 901 (1994).

[99] S. J. Brodsky, P. Hoyer, C. Peterson, and N. Sakai, Phys. Lett. **93B**, 451 (1980); S. J. Brodsky, C. Peterson, and N. Sakai, Phys. Rev. D **23**, 2745 (1981).

[100] S. J. Brodsky, P. Hoyer, A. H. Mueller, and W.-K. Tang, Nucl. Phys. **B369**, 519 (1992).

[101] R. C. Hwa and M. S. Zahir, Z. Phys. C **20**, 27 (1983).

[102] E. V. Bugaev and E. S. Zaslavskaya, Institute for Nuclear Research, Academy of Sciences of the USSR, Report No. Π-0400, 1985 (unpublished).

[103] S. J. Brodsky, J. F. Gunion, and D. E. Soper, Phys. Rev. D **36**, 2710 (1987).

[104] EMC Collaboration, J. J. Aubert *et al.*, Phys. Lett. **110B**, 73 (1982); Nucl. Phys. **B213**, 31 (1983).

[105] Fermilab E653 Collaboration, K. Kodama *et al.*, Phys. Lett. B **284**, 461 (1992).

[106] J. Kuti and V. J. Weisskopf, Phys. Rev. D **4**, 3418 (1971).

[107] E. Takasugi and X. Tata, Phys. Rev. D **26**, 120 (1982).

[108] ISR Collaboration, M. Basile *et al.*, Lett. Nuovo Cimento **30**, 481 (1981); **30**, 487 (1981).

[109] R. C. Hwa, Phys. Rev. D **22**, 1593 (1980).

[110] E. M. Levin and L. L. Frankfurt, Pis'ma Zh. Éksp. Teor. Fiz. **2**, 65 (1965) [JETP Lett. **2**, 108 (1965)]; H. K. Lipkin and F. Sheck, Phys. Rev. Lett. **16**, 71 (1966).

[111] G. Berlad, A. Dar, and G. Eilam, Phys. Rev. D **22**, 1547 (1980).

[112] WA82 Collaboration, M. Adamovich *et al.*, Phys. Lett. B **284**, 453 (1992).

[113] R. Vogt, S. J. Brodsky, and P. Hoyer, Nucl. Phys. **B383**, 643 (1992).

[114] BIS-2 Collaboration, A. N. Aleev *et al.*, Yad. Fiz. **56**, 147 (1993) [Phys. At. Nucl. **56**, 1235 (1993)].

[115] G. t'Hooft, Nucl. Phys. **B72**, 461 (1974); G. Veneziano, *ibid.* **B74**, 365 (1974); M. Ciafaloni, G. Machesini, and G. Veneziano, *ibid.* **B98**, 472 (1975).

[116] LEBC-EHS Collaboration, M. Aguilar-Benitez *et al.*, Phys.

Lett. B **201**, 176 (1988); Z. Phys. C **40**, 321 (1988).

[117] A. B. Kaidalov, Yad. Fiz. **33**, 1369 (1981) [Sov. J. Nucl. Phys. **33**, 733 (1981)].

[118] A. J. Buras, Nucl. Phys. **B109**, 373 (1976); K. Yamada, Phys. Rev. D **22**, 1676 (1980). For a recent review of the experimental measurements and theoretical descriptions of semileptonic decays of charmed particles, see J. D. Richman and P. R. Burchat, Rev. Mod. Phys. **67**, 893 (1995).

[119] We have in mind the data for the vertical muon flux. Notice that our calculations for the near-horizontal flux are in good agreement with the direct data from the two large magnetic spectrometers MUTRON [18] and DEIS [19] up to about 20 TeV/c irrespective of the PM flux model (the near-horizontal muon flux is considerably less sensitive to the PM contribution than is the vertical spectrum).

[120] Cf. the outputs of the earlier KGF data analyses performed in Refs. [59] and [88].

[121] G. T. Zatsepin and E. D. Mikhalchi, J. Phys. Soc. Jpn. **17**, Suppl. A-III, 365 (1962); V. I. Gurentsov, G. T. Zatsepin, and E. D. Mikhalchi, Yad. Fiz. **23**, 1001 (1976) [Sov. J. Nucl. Phys. **23**, 527 (1976)].

[122] N. Takahashi, H. Kujirai, A. Adachi, N. Ogita, and A. Misaki, Uchuusen-Kenkyuu **28**, 120 (1984).

[123] E. V. Bugaev, V. A. Naumov, and S. I. Sinegovsky, Yad. Fiz. **41**, 383 (1985) [Sov. J. Nucl. Phys. **41**, 245 (1985)]; Izv.

Akad. Nauk SSSR, Ser. Fiz. **49**, 1389 (1985) [Bull. Acad. Sci. USSR, Phys. Ser. **49**, 146 (1985)].

[124] V. A. Naumov, S. I. Sinegovsky, and E. V. Bugaev, in *Proceedings of the 2nd NESTOR International Workshop* [56], p. 119; Yad. Fiz. **57**, 439 (1994) [Phys. At. Nucl. **57**, 412 (1994)].

[125] E. V. Bugaev, V. A. Naumov, S. I. Sinegovsky, A. Misaki, N. Takahashi, and E. S. Zaslavskaya, in *Proceedings of the 3rd NESTOR International Workshop* [16], p. 268; in *Proceedings of the RIKEN International Workshop on Electromagnetic and Nuclear Cascade Phenomena in High and Extremely High Energies*, Tokyo, Japan, 1993, edited by M. Ishihara and A. Misaki (RIKEN, Tokyo, 1994), p. 264.

[126] R. P. Kokoulin and A. A. Petrukhin, in *Proceedings of the 22nd International Cosmic Ray Conference* [68], Vol. 4, p. 536; N. P. Longley, in *Proceedings of the 25th International Cosmic Ray Conference* [46], Vol. 6, p. 413.

[127] A. A. Lagutin, V. A. Litvinov, and V. V. Uchaikin, *Theory of Sensitivity in Cosmic-Ray physics* (Altai University Press, Barnaul, 1995); C. Badino, W. Fuglione, E. Kemp, and A. Turtelli, in *Proceedings of the 25th International Cosmic Ray Conference* [46], Vol. 6, p. 417.

[128] The data presented in Fig. 14 have been kindly provided by the LVD Collaboration in advance of publication.